Research on Engineering Structures & Materials
www.jresm.org
Research Group

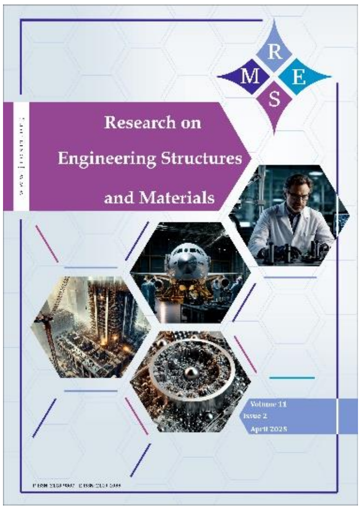

Recent trends and open challenges in battery management systems: A comprehensive review with hardware-in-the-loop simulation for electric vehicle applications

Sourav Dutta, Saikat Adikari, Tushar Debnath, Rudra Sankar Pal, Kumar Amitabh, Madhur Chauhan, Anik Goswami, Pradipta Ghosh

Online Publication Date: 10 March 2026
URL: http://www.jresm.org/archive/resm2026-1349en1119rv.html
DOI: http://dx.doi.org/10.17515/resm2026-1349en1119rv

Journal Abbreviation: *Res. Eng. Struct. Mater.*

To cite this article
Dutta S, Adikari S, Debnath T, Pal R S, Amitabh K, Chauhan M, Goswami A, Ghosh P. Recent trends and open challenges in battery management systems: A comprehensive review with hardware-in-the-loop simulation for electric vehicle applications. *Res. Eng. Struct. Mater.*, 2026; 12(4): 2539-2570.

Research on Engineering Structures & Materials
www.jresm.org
MIM Research Group

Review Article

Recent trends and open challenges in battery management systems: A comprehensive review with hardware-in-the-loop simulation for electric vehicle applications

Sourav Dutta [*,1,2,a], Saikat Adikari [3,4,c], Tushar Debnath [2,c], Rudra Sankar Pal [1,d], Kumar Amitabh [2,e], Madhur Chauhan [2,f], Anik Goswami [1,5,g], Pradipta Ghosh [2,6,h]

[1]*Department of Electrical Engineering, IIT (Indian School of Mines) Dhanbad, Jharkhand, India*
[2]*Department of Electrical Engineering, NIT Mizoram, Aizawl, Mizoram, India*
[3]*Advanced Technology Development Centre, IIT Kharagpur, West Bengal, India*
[4]*Senior Functional Safety Engineer, FEV India*
[5]*School of Electrical Engineering, Vellore Institute of Technology, Chennai, India*
[6]*Department of Electrical and Electronics Engineering, Swami Vivekananda Institute of Science and Technology, West Bengal, India*

Article Info

Article History:

Received 19 Nov 2025
Accepted 05 Mar 2026

Keywords:

Battery management system;
Electric vehicle;
Energy storage systems;
Lithium ion battery;
State of health;
State of charge;
State of estimation;
State of energy;
State of power;
State of function;
State of life

Abstract

The paper highlights a novel approach that provides a system-level Battery Management System (BMS) review for electric vehicles (EVs), particularly with respect to Hardware-in-the-Loop (HIL) validation. This bridges the gap between algorithmic research and real-time BMS testing. Energy storage system (ESS) technology remains a challenge for EVs, expected to dominate future transport. A sophisticated BMS is crucial for monitoring battery health, ensuring safety, and extending lifespan. Using voltage, current, and temperature measurements, the BMS estimates parameters like SOC, SOH, impedance, capacity, power fade, and remaining life, vital for safety devices, charge balancing, thermal management, and optimal charging. Resilient BMS includes precise characterization, reliable estimation, and effective control. Development requires comprehensive testing of analog I/O and embedded code; HIL simulations offer advantages over traditional testing, providing reproducibility, efficiency, and safety, especially for ranges beyond normal limits. HIL is invaluable for early development, particularly for logic and fault testing. This review covers Li-ion battery modeling using experimental data, implemented in real time with Opal-RT HIL. A scalable model with electronic devices enables thorough BMS testing, demonstrating the validation of key functions, including protection, temperature, current, voltage monitoring, and cell balancing. HIL simulation is essential for modern BMS development.

1. Introduction

A quarter of the world's energy use is attributed to gasoline-powered cars [1]. When EVs take their position in the not-so-distant future, rechargeable batteries may help. Rechargeable batteries (RBs) are now used in power tools, home appliances, renewable energy systems, portable electronics, and airplanes in addition to electric cars. The performance of RBs has been a focus for the US, Japan, China, and Germany in recent years, with notable progress made in this area [2]. Many energy storage technologies have gained acceptance for use in transportation in recent years, comprising

*Corresponding author: souravduttaphd@gmail.com
[a]orcid.org/0009-0003-9374-4075; [b]orcid.org/0000-0003-2048-624X; [c]orcid.org/0000-0003-0590-2292; [d]orcid.org/0000-0001-7279-1014; [e]orcid.org/0009-0005-8655-2686; [f]orcid.org/0000-0003-0442-0312; [g]orcid.org/0000-0002-1399-0424; [h]orcid.org/0000-0002-0051-4859
DOI: http://dx.doi.org/10.17515/resm2026-1349en1119rv

Zinc-bromide flow battery (ZBFB), Lead-acid, Lithium-ion (Li-ion), Sodium nickel chloride (NaNiCl), Vanadium redox flow battery (VRFB), Nickel-Cadmium (NiCd), and Sodium sulphur (NaS) batteries [3]. The Li-ion battery is one of the best, offering a long lifespan, high power density, low discharge rate, high efficiency, and high dependability [4]. Furthermore, the costs of Li-ion batteries are decreasing, making them more attractive in the EV sector [5], and as a result, the market for Li-ion batteries is expanding [6]. Thermal runaway, an irreversible chemical process triggered by several factors, including overvoltage and extreme temperatures, can occur in lithium-ion batteries. Thermal runaway and other safety-related issues are more likely to occur when the battery needs to be fast-charged, which is particularly important in the use of electric vehicles [7-8]. Various factors impact the effectiveness of energy storage in batteries; in particular, the use of EVs aims to maximize efficiency. Charge efficiency, for instance, is the proportion of the total energy required for charging [9]; high charging demands result in significant energy loss in the form of heat. Appropriate SOC estimation algorithms ensure that efficiency is enhanced by assisting in the design of minimal battery-pack configurations based on specific criteria. The dependability, efficiency, and safety of a battery-powered system are ensured by a Battery Management System (BMS). BMS algorithms aim to improve battery efficiency in multiple ways; optimal charging algorithms aim to minimize heat waste and reduce degradation of the battery's state of health. One typical cause of safety and reliability problems with Li-ion batteries is short-circuited cells, which can also result from individual cells in a battery pack becoming unbalanced over time [10-12]. Energy Storage System (ESS) technology poses significant challenges for electric vehicles (EVs), primarily due to trade-offs in Li-ion battery chemistries regarding energy density, power rating, safety, cost, and lifespan [13-15]. While high-energy-density batteries like NMC and NCA offer longer ranges [16-17], they degrade more quickly and present thermal safety risks compared to LFP batteries [18-19]. Battery degradation is influenced by complex factors, such as temperature and charging or discharging rates [20], with fast charging exacerbating the issue [21]. Additionally, the environmental impact of Li-ion batteries, including the use of critical materials and low recycling rates [22], underscores the need for balanced advancements in battery technology [23], control strategies, and sustainable practices [24].

We may effectively employ HIL tests to verify these operations. The benefits of several rechargeable batteries and BMS technologies—such as heat management, SOH, and SOC estimations—are presented in this overview. Next, a thorough description of the BMS HIL test procedure in the EV application was given. Future directions for research have also been discussed. So, the novelty and the contribution of the work are mentioned as follows;

- Heat management is discussed and verified for improving the battery management system.
- Estimates like SOH and SOC for rechargeable batteries are presented.
- A thorough description of the BMS HIL test is presented for the EV application.

The paper aligns strongly with several Sustainable Development Goals, particularly SDG 7: Affordable and Clean Energy, SDG 9: Industry, Innovation and Infrastructure, and SDG 13: Climate Action, by advancing the development of efficient and reliable BMS for EVs. Through the use of HIL simulation, the study promotes innovative and safe testing methods that enhance battery performance, lifespan, and safety, which are critical for the widespread adoption of energy storage systems and clean transportation. Improved monitoring and estimation of battery parameters such as state of charge and health contribute to optimized energy use and reduced resource waste, supporting SDG 12: Responsible Consumption and Production. Additionally, by enabling more dependable electric vehicles, the research contributes to cleaner urban mobility and supports SDG 11: Sustainable Cities and Communities, ultimately helping reduce carbon emissions and combat climate change.

2. Review of Research Findings

2.1 Energy Storage Systems

A motor, a power converter, a mechanical transmission, and an ESS comprise the main parts of an electric vehicle. Globally, various energy storage systems are currently available, including lead-acid, VRFB, ZBFB, NaS, NaNiCl, and Li-ion. The table below lists all the features of the batteries previously discussed.

Lithium-ion batteries have the highest power and energy densities, whereas VRFB batteries have the longest life cycles, as shown in the table above. Regarding cost, nominal voltage, and life cycle, Li-ion batteries are ideal for electric vehicle applications. The spider chart for the chemistries of the various cells is displayed in Figure 1 to facilitate easy understanding and comparison [26].

Table 1. Characteristics of the various types of energy storage systems [25]

Battery type	Energy Density (Wh/L)	Power Density (W/L)	Nominal Voltage (V)	Life cycle	DOD (%)	Round-trip efficiency (%)	Estimated Cost USD/kWh
Lead acid	50-80	10-400	2.0	1500	50	82	105-475
NaS	140-300	140-180	2.08	5000	100	80	263-735
NaNiCl	160-275	150-270	-	3000	100	84	315-488
NiCd	60-150	80-600	1.3	2500	85	83	-
VRFB	25-33	1-2	1.4	13000	100	70	315-1050
ZBFB	55-65	1-25	1.8	10000	100	70	525-1680
Li-ion	200-400	1500-10000	4.3	10000	95	96	200-1260

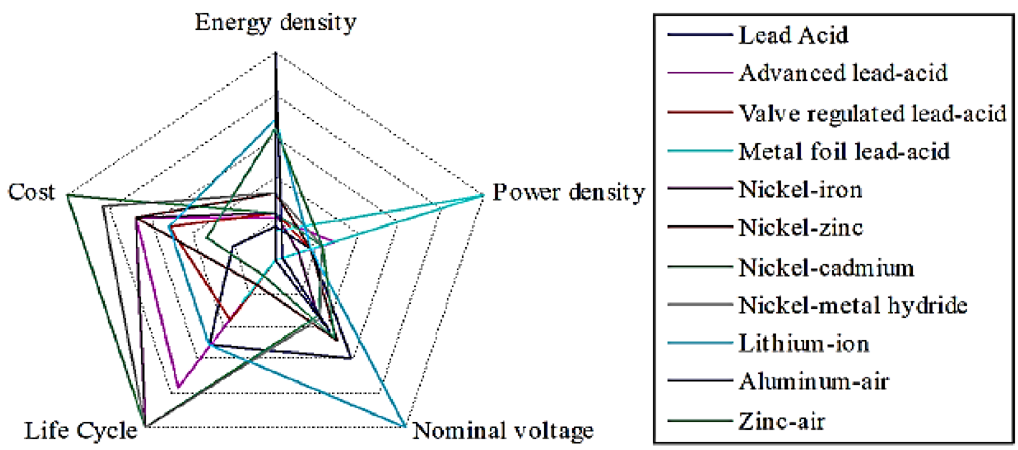

Fig. 1. Spider chart of chemistries of various cells [26-28]

2.1.1 Lithium-Ion Battery

A Lithium-ion cell is composed of a separator, two current collectors, a cathode (negative electrode), an anode (positive electrode), and both. Li-ion manganese oxide (LMO), Li-iron phosphate (LFP), Li-Sulphur (LiS), Li-Titanate Oxide (LTO), or Li-nickel-manganese-cobalt oxide (LNMC) are the materials generally found in the anode, whereas graphite typically acts as the negative electrode. Ethyl or diethyl carbonate can be used as the electrolyte. As negative and positive current collectors, respectively, copper and aluminium are employed.

Table 2. Comparison of several Li-ion battery types [2,27]

Type	Energy Density (Wh/kg)	Power Density (W/kg)	Life Cycle	Estimated Cost (USD/kWh)	Safety	Maturity
LMO	160	200	2000	360	Good	Commercial
LFP	120	200	2500	360	Good	Commercial
LNMC	200	200	2000	360	Good	Commercial
LTO	70	1000	10000	860	Good	Demo
LiS	500	-	100	-	Good	R&D Stage

The following Table [2,] compares several Li-ion battery types. Lithium-ion batteries are the best choice for EVS; however, they must still possess a long-life cycle, improved performance, better thermal control, and lower capital costs.

2.1.2 Battery Management System (BMS)

The architecture and design of the BMS are dealt with at a conceptual level in the current work. However, a comprehensive system-level embedded BMS architecture, comprising sensing layers, real-time estimation modules, control logic, safety monitoring, and communication interfaces, has not been fully developed within the current scope. The current work provides the necessary functional building blocks and requirements for such development, while hardware-software co-design and real-time development will be carried out in future work. In the current study, the parameters of the equivalent circuit model (ECM) and thermal model were primarily taken from the literature and datasheet values, and were adapted for HIL simulation compatibility, rather than fully characterized through experimental parameter identification and optimization. The experimental identification and optimization of ECM and thermal model parameters using laboratory test data (such as pulse testing, Hybrid Pulse Power Characterization (HPPC), and thermal cycling) will be considered in future work.

A robust and advanced BMS is needed when ESS has adequately matured. The BMS consists of three main components in EVs: controls, sensors, and actuators. An efficient BMS performs the following primary tasks. i) protects the battery; ii) operates within safe limits for voltage, current, and temperature; and iii) precisely measures and evaluates the battery's state [28].

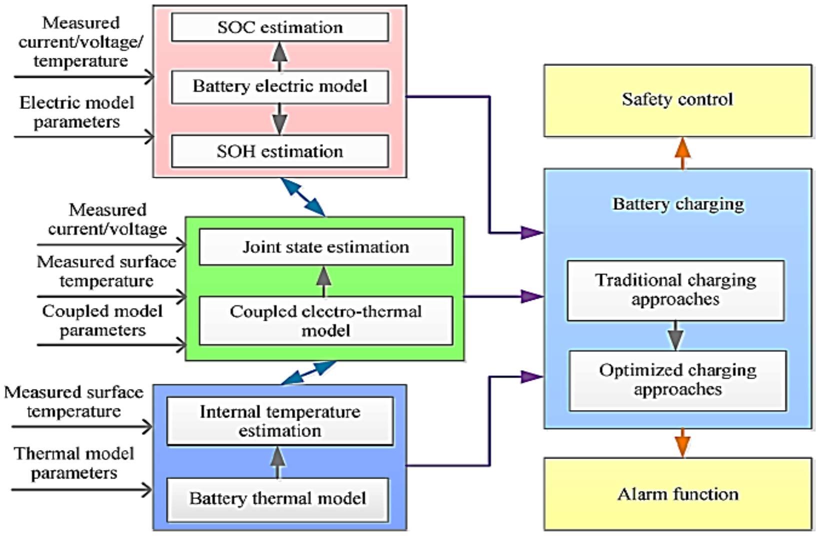

Fig. 2. Relation of key technologies in the BMS [29]

2.1.3 State of Health Estimation

In this study, thermal management is not explicitly included as the focus is on developing a framework for electrical behavior modelling and estimation. While thermal phenomena are crucial for battery safety and other functions in electric vehicles, incorporating electro-thermal modelling would complicate the system. This work lays the groundwork for future complete BMS implementations that will address thermal effects.

Degradation of batteries results in a reduction in their energy storage capacity and fast charging/discharging performance. The degree of aging of batteries can be assessed quantitatively using the SOH index. Model-based and experimental analytic methods are the two groups into which SOH estimation techniques can be divided [30], as illustrated in Figure 3 below. The battery SOH has no specific definition. A broad explanation of battery SOH is as follows:

$$SOH(t) = SOH(t_0) + \int_{\tau=t_0}^{t} \partial_{func}(I, T, SOC, others) d\tau \quad (1)$$

where SOH (t_0) represents the initial battery SOH, an aging rate function is highly dependent on several variables, including temperature, current, and SOC. Other variables that SOH represents include mechanical vibrations and over-potential.

The capacity/energy measurement test is suitable for bench tests or stable conditions, as it requires precise data collection and high integrity of the charging and discharging processes. Ohmic resistance measurement is a simple, accurate, and real-time method that requires pulse voltage and current. Impedance measurement requires an electrochemical workstation or AC excitation apparatus [31]. Electrochemical Impedance Spectroscopy (EIS) can yield distinctive parameters for calibrating SOH. A multi-step derivation technique indirectly estimates internal resistance or capacity by analyzing various health indicators, including film resistance, the capacity-OCV-SOC response surface, the voltage response trajectory, the incremental capacity curve, and ultrasonic wave response. Battery SOH can be assessed by combining multiple health parameters.

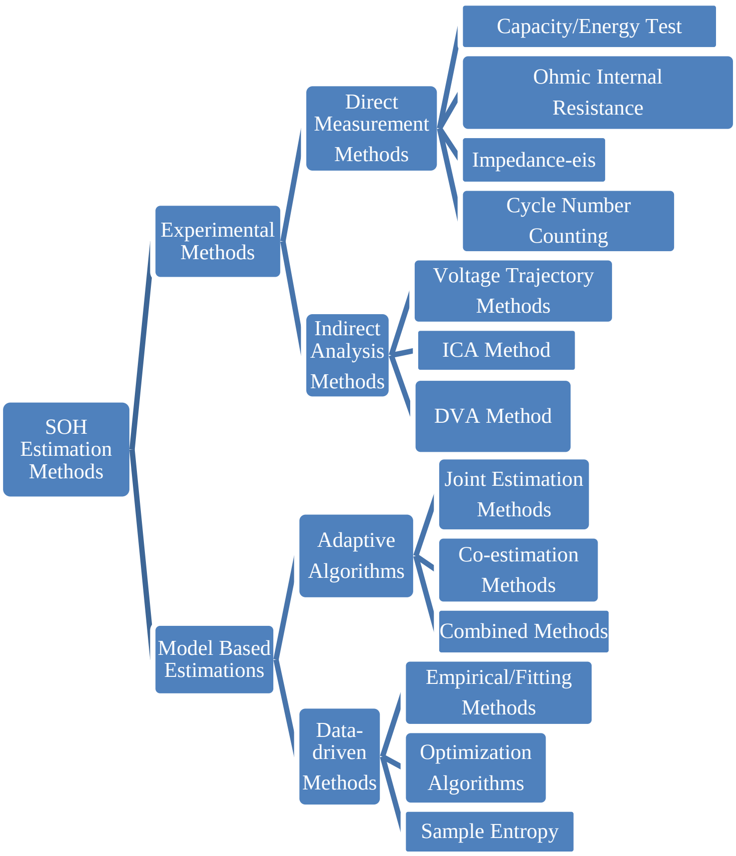

Fig. 3. Flow chart showing estimation methods of SOH [31]

The empirical/fitting approach is a data-driven method for estimating battery life based on available aging data. It uses polynomial, exponential, power law, logarithmic, and trigonometric functions, often computing quickly and with minimal computational complexity. The Arrhenius equation is used to model temperature-dependent processes, such as diffusion coefficients and creep rates, demonstrating its effectiveness in SOH calculations [32]. The Arrhenius equation can also be used to describe the temperature-dependent aging rate of batteries, as shown in the following equation;

$$\frac{dC}{dn} = \wedge\, e^{-\frac{\Delta E}{R_g T}} = \wedge\, e^{-\frac{\lambda}{T}} \quad (2)$$

Where $\frac{dC}{dn}$ represents the change rate of cell capacity relative to the aging cycle, $\wedge$ indicates the pre-exponential factor, R_g is defined as the general gas constant, i.e., 8.314 J/(mol K), ΔE denotes the activation energy, in units of J/mol, and T refers to the absolute temperature, in units of K. $\wedge$ and λ $\frac{\Delta E}{R_g}$ represent two unknown parameters needing to be calibrated. Integrating Eq. gives;

$$C_r = -\wedge n_c e^{-\frac{\lambda}{T}} \tag{3}$$

Where C_r indicates the threshold of capacity reduction, indicating the degradation of the cell, and n_c denotes the cycling life of the cell. Two different temperature points, T_1 and $T_2 (T_1 > T_2)$, were selected.

$$\Delta n_c = \frac{C_r}{\Lambda}\left(e^{-\frac{\lambda}{T_2}} - e^{-\frac{\lambda}{T_1}}\right) \tag{4}$$

The influence of temperature on the cell lifetime is described quantitatively by Δn_c, which is defined as the lifetime gap between two temperature levels. The Arrhenius equation can be used to evaluate the battery's SOH at several temperatures once its characteristics have been determined.

The current method for estimating SOH differs from those used in neural networks or machine learning topologies. Neural networks are used for voltage curve estimation, while machine learning topology utilizes changes in temperature, current, and internal circuit characteristics. Support vector machine approaches classify SOH; partial charging voltage curves are estimated. Charging time and capacity required for online estimation. The terminal voltage under the hybrid pulse power characterization current profile is identified using a sample entropy approach [33-37].

2.1.4 Optimal Charging

The safety mechanisms in the system include fault detection, isolation, protection logic, and abuse handling, ensuring reliable operation of EV components under abnormal conditions. However, a lack of description regarding the fault conditions tested in HIL simulations hinders understanding of the mechanisms' effectiveness during actual faults. Battery charging using modern technology is outdated, time-consuming, and insecure compared to gasoline [38]. Optimal charging algorithms (OCA) have gained attention, with the continual trickle-current-based strategy being a popular technique [39]. However, shortening the charging time by increasing the charging current results in the terminal voltage exceeding the safety threshold [40-41]. When the terminal voltage reaches a threshold, the initial higher current needs to be reduced [42].

The constant-current constant-voltage (CC-CV) strategy is a popular method for quick charging, offering shorter charging times and longer battery life cycles [43]. Taguchi-based battery charging techniques use orthogonal arrays for methodical solution selection [44-45]. Boost charging delivers high current to depleted batteries, while pulse-charging techniques require brief rest intervals or intentional discharging phases [46-48]. Battery charging profile optimization can be achieved using soft-computing techniques, such as an ant colony method and a universal voltage protocol [49-50]. These methods aim to improve cycle life and charging efficiency by establishing a specific charging profile based on the battery's SOH [51]. An optimization method, utilizing a cost function that combines energy loss and time-to-charge, has been employed to determine the optimal charging plan [52-53]. Alternative methods include data mining, neural networks, and genetic algorithm-based tactics, as well as grey-predicted charging systems [54-56].

In charging optimization, advantage is taken of battery models that were developed in earlier studies. The effects of temperature, health state, and charging-voltage threshold on charging outcomes are examined for lithium nickel manganese cobalt oxide (LiNMC) and lithium iron phosphate ($LiFePO_4$) batteries [51]. Constant-current-constant-voltage (CC-CV) charging is considered the most popular method for charging lithium-ion batteries. However, the battery's performance and lifespan are affected by excessive temperature increases during the CC stage. It follows that an extension of the CV process is required. An ideal charging algorithm based on the Genetic Algorithm (GA) is proposed below to minimize the charging temperature increment while maintaining a reasonable charging time. The correlation equation can be expressed as follows if the battery temperature is measured following a 0.1% SOC increment.

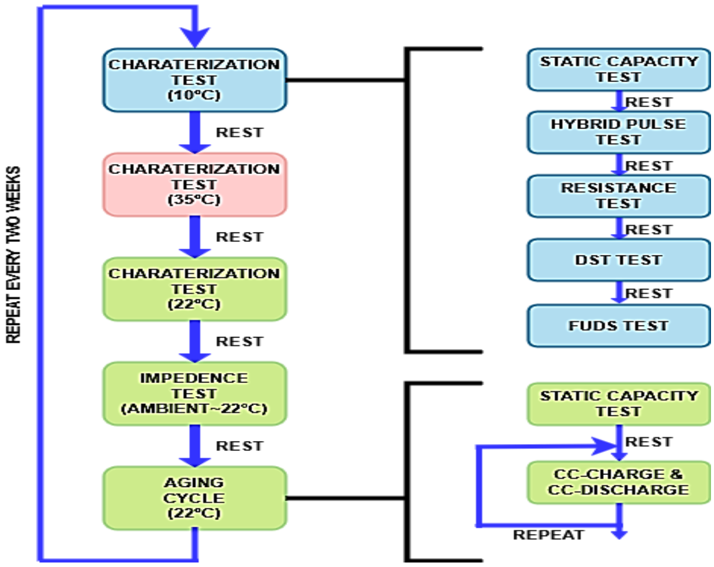

Fig. 4. The test chart for the collection of battery data. [52]

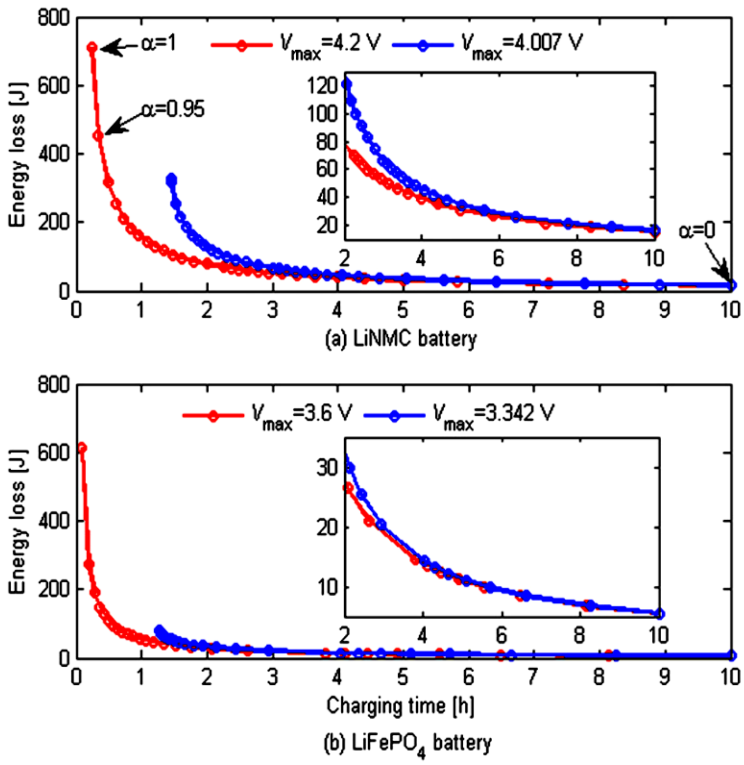

Fig. 5. Pareto charts of the multi-objective optimization for the two types of Li-ion batteries at 22°C: (a) LiNMC battery; (b) $LiFePO_4$ battery, where α is the weighting factor that takes values from 0 to 1, which reflects the proportionate importance of the two objectives. [52]

$$T(S) = T(S - 0.1\%) + \frac{I^2 . R_0 + I . V_p - A . h(T(S - 0.1\%) - T_{air})}{mC} \tag{5}$$

where S is SOC, I is charging current, R_0 is the Ohmic resistance of the battery, V_p is polarization voltage, h is the heat transfer coefficient, T_{air} is ambient temperature, m is the mass of the battery, A is the surface area of the battery, and finally C is the specific heat capacity.

We define $\beta(I) = (I^2.R_0 - I.V_p + A.h.T_{air})/mC$ and $\alpha = 1 - A.h/mC$

Now, the above equation can be written as

$$T(S) = \alpha.T(S - 0.1\%).(S - 0.1\%) + \beta(I) \tag{6}$$

The solution of the equation can be calculated. The solution of the equation can be calculated.

$$T(S) = \alpha^k.T(0) + \sum_{l=0}^{k} \alpha^{k-1-l}.\beta(I_{l+1}) \tag{7}$$

Where $k = \frac{s}{0.1\%}$

Now R_0 and V_p need to be appropriately estimated. These parameters can be calculated by the Hybrid Pulse Power Characterization (HPPC) test and the Equivalent Circuit Model (ECM).

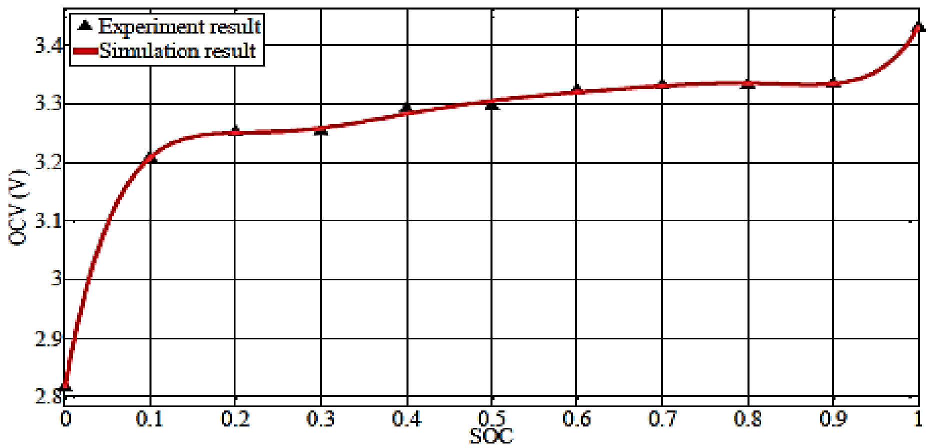

Fig. 6. Measured OCV curve with different SOC values [48]

Fig. 6 shows the measured OCV curve with different SOC values. The relation between OCV and battery SOC can be standardized as follows –

$$f_{OCV}(S) = P_1S^7 + P_2S^6 + P_3S^5 + P_4S^4 + P_5S^3 + P_6S^2 + P_7S + P_8 \tag{8}$$

Similarly, this figure shows the measured ohmic resistance with changing SOC. The relationship can be formulated as follows;

$$f_{R_0}(S) = a_1S^5 + a_2S^4 + a_3S^3 + a_4S^2 + a_5S + a_6 \tag{9}$$

Polarization voltage can be calculated as,

$$V_P = V_t - f_{OCV}(S) - I.f_{R_0}(S) \tag{10}$$

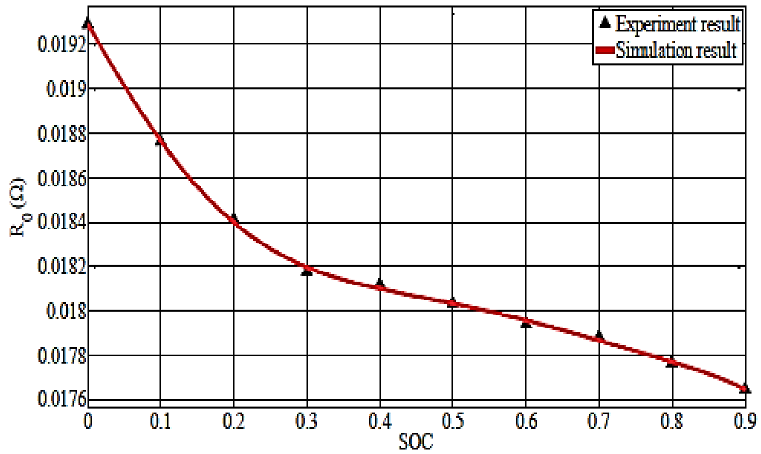

Fig. 7. Plot between battery ohmic resistance and SOC [48]

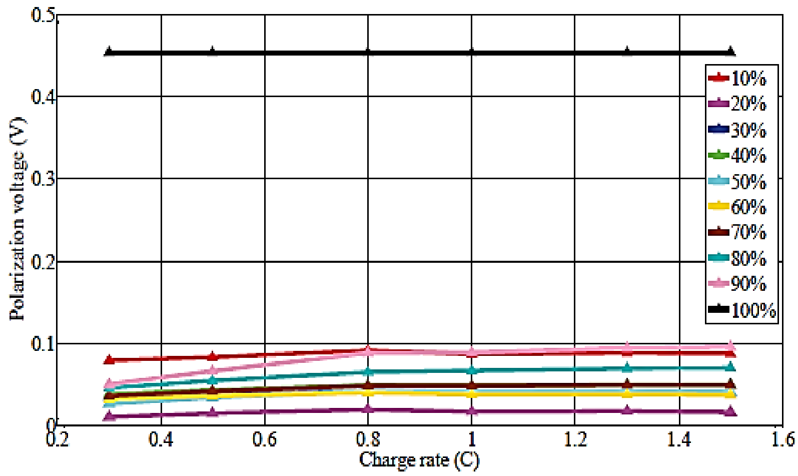

Fig. 8. Polarization voltage versus charging rate with different SOC levels [48]

The difference between the end and beginning temperatures can be characterized as the objective function, considering the influence of battery temperature and the battery charging temperature model. Assuming that the charging process takes n steps to attain the target SOC, the initial temperature T(0) is T_0, the final temperature T(n) is T_n, and therefore the temperature increment is $\Delta T = T_n - T_0$

$$J = T_n - T_0 = \alpha^k.T(0) + \sum_{l=0}^{k} \alpha^{k-1-l}.\beta(I_{l+1}) - T_0 \tag{11}$$

$$= (\alpha^k - 1).T_0 + \sum_{l=0}^{1000n} \alpha^{1000n-1-l}.\beta(I_{l+1}) \tag{12}$$

The optimization goal is to determine the optimal charging current, I1, to minimize the objective function, J, during the charging process. Battery charging time is a significant index to evaluate a charging strategy, which is different as the time taken to charge the battery from the initial SOC. $S_{initial}$ to target SOC, S_{target}. Now, the sum of the charging time at each step, i.e. $t_{total} = \sum_{l=1}^{n} \frac{\Delta C_l}{I_l}$. Where ΔC_l denotes the value at the different steps of the charging capacity.

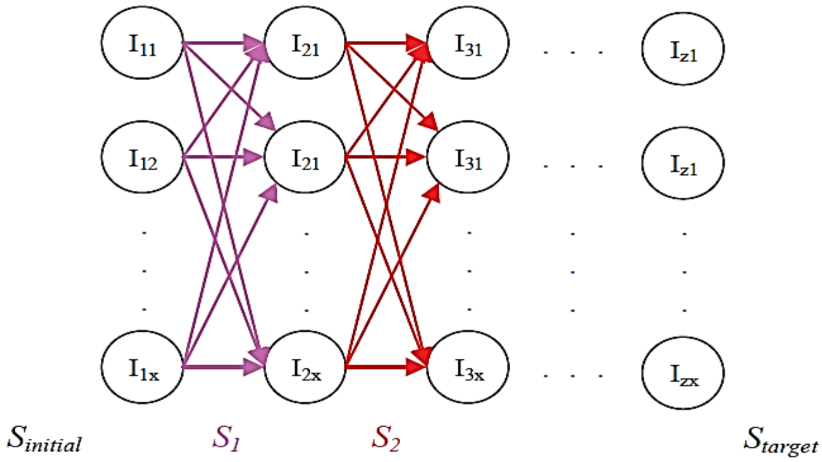

Fig. 9. Temperature variation profile [48]

The total charging time is lower than the constant current charging strategy. Therefore $t_{total} \leq t_{cc}$, Where t_{cc} refers to the charging time required when charging the battery at a constant current, as specified by the battery manufacturer. The charging current and voltage should be lower than the maximum permissible charging current and the maximum cut-off voltage, respectively, *i.e.* $V_t \leq V_{cut}$; $I_t \leq I_{max}$.

The implementation process is shown in the figure below. When charging from $S_{initial}$, it is assumed that *x* charging values and *z* step charging stages exist; therefore, x^z types of current combinations are obtained. Each type of charging current combination corresponds to a specific charging temperature increment mode; the minimum temperature increment current combination is selected as the optimal charging current.

2.1.5 Battery Thermal Management

Thermal behaviour, including temperature, is crucial for battery performance and lifespan in electric vehicles (EVs) [57]. Models capture this, including data-driven, reduced-order thermal, as well as heat generation and heat transfer, which explain the non-uniformity within batteries. Three widely used methods for evaluating the generation of heat in batteries are presented in Eq. (13) and are utilized extensively in real-time applications [58–61].

$$\begin{cases} Q_1 = RI^2 \\ Q_2 = I(V - OCV) \\ Q_3 = I(V - OCV) + IT\dfrac{dOCV}{dT} \end{cases} \tag{13}$$

where R is the internal resistance of the battery, I and V represent the current and voltage of the battery, respectively, OCV represents the open circuit voltage of the battery, Q_1 represents the heat generation of the battery which is mainly due to the huge current flowing through the internal resistance of the battery, Q_2 represents the heat generation of the battery due to the over-potentials across the RC network, Q_3 represents the heat generation of the battery due to both the entropy change and Joule's heating.

The three primary methods of heat transport that occur both inside and outside of batteries are heat convection, heat conduction, and heat radiation. In order to investigate the geometrical current and heat distribution within Li-ion batteries, Guo *et al.* [62] created a three-dimensional distributed-parameter heat transfer model, which is depicted as follows:

$$\frac{\partial \rho C_p T_{3C}}{\partial t} = -\nabla(k_{3C}\nabla T_{3C}) + Q \tag{14}$$

It can also be expressed as [51]

$$\frac{\partial \rho C_p T_{3C}}{\partial t} = -\frac{\partial}{\partial x}\left(k_x \frac{\partial T_{3C}}{\partial x}\right) - \frac{\partial}{\partial y}\left(k_y \frac{\partial T_{3C}}{\partial y}\right) - \frac{\partial}{\partial z}\left(k_z \frac{\partial T_{3C}}{\partial z}\right) + Q \tag{15}$$

Where the battery density is represented by ρ, the battery heat capacity is denoted by C_p, k_{3C} is the coefficient of battery thermal conductivity (along three dimensions: k_x k_y k_z), Q means battery heat generation. A simplified one-dimensional heat conduction model can be created [63-64] in the following manner, assuming that the battery temperature distribution inside each layer plane is uniform and that only one dimension of battery heat conduction (e.g., the x dimension) is taken into consideration.

$$\frac{\partial \rho C_p T_{1C}}{\partial t} = -\frac{\partial}{\partial x}\left(k_x \frac{\partial T_{1C}}{\partial x}\right) + Q \tag{16}$$

The temperature distribution inside the battery can be described by the three-dimensional heat transfer models, which can be used to identify potential hot spots, particularly in applications involving substantial heat generation. A one-dimensional heat transfer model can represent the temperature gradient in a single direction. These heat transfer models are primarily used in offline simulations because their computational overhead is frequently too high for real-time applications.

Considering that the primary mechanism of heat transport is conduction, the heat generation is dispersed equally inside the battery, and the interior and exterior temperatures of the battery are both constant, a well-liked two-stage thermal model for battery cells [65-67] can be developed as follows-

$$\begin{cases} C_{q1} dT_{in}/dT = k_1(T_{sh} - T_{in}) + Q \\ C_{q2} dT_{sh}/dt = k_1(T_{in} - T_{sh}) + k_2(T_{amb} - T_{sh}) \end{cases} \tag{17}$$

where T_{in} and T_{sh} stand for internal temperature and surface temperature of the battery, respectively, T_{sh} means the ambient temperature around the battery, $C_{q1,}$ and C_{q2} stands for the thermal capacities of the battery interior and surface, k_1 stands for the heat conduction between the battery surface and the interior, k_2 stands for the heat conduction between the ambiance and the battery surface. Reduced-order thermal models have been developed for controlling battery thermal management, identifying heat generation and transport components. These models are based on a computational fluid dynamics (CFD) model, which has lower computation costs and similar findings to the CFD model. This approach helps in controlling battery thermal management [68-70].

2.1.6 State of Charge Estimation

SOC represents a battery's remaining capacity relative to its overall capacity, with 100% indicating a fully charged battery and 0% indicating a discharged one [13]. SOC assessment is crucial for safe operation. There are direct estimation techniques and model-based methods, with OCV and Ah methods being the primary methods. The Ah method is a general and simple method to calculate SOC [71-72], which is illustrated as follows,

$$SOC(k)=SOC(k_0) + \int_{k_0}^{k} \eta I(t) dt / C_n \tag{18}$$

Where SOC(k_0) is the known initial SOC, η stands for the efficiency of battery charging or discharging, C_n stands for the battery nominal capacity, $I(t)$ is the current value, which is positive during charging and negative during discharging. The Ah technique is a popular choice for monitoring charging and discharging current; however, its accuracy is influenced by mistake accumulation and real-time challenges, especially when the battery's charge level is between 10% and 90% [71-72].

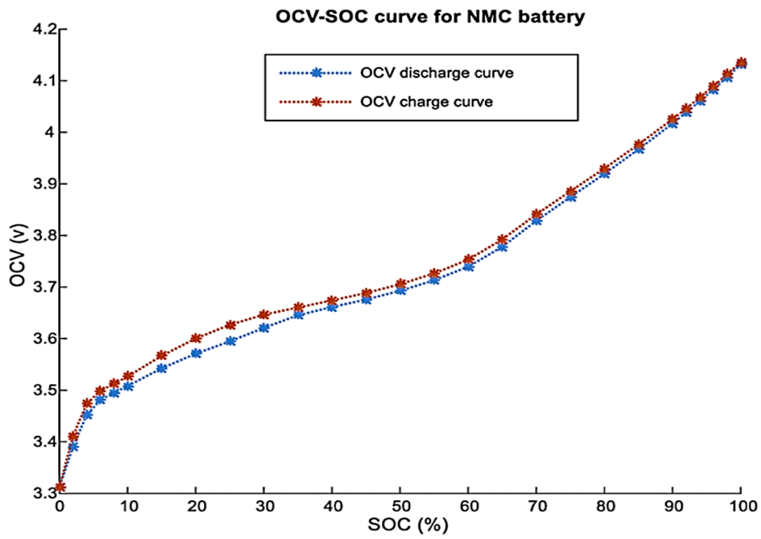

Fig. 10.Relationship between the battery OCV and SOC

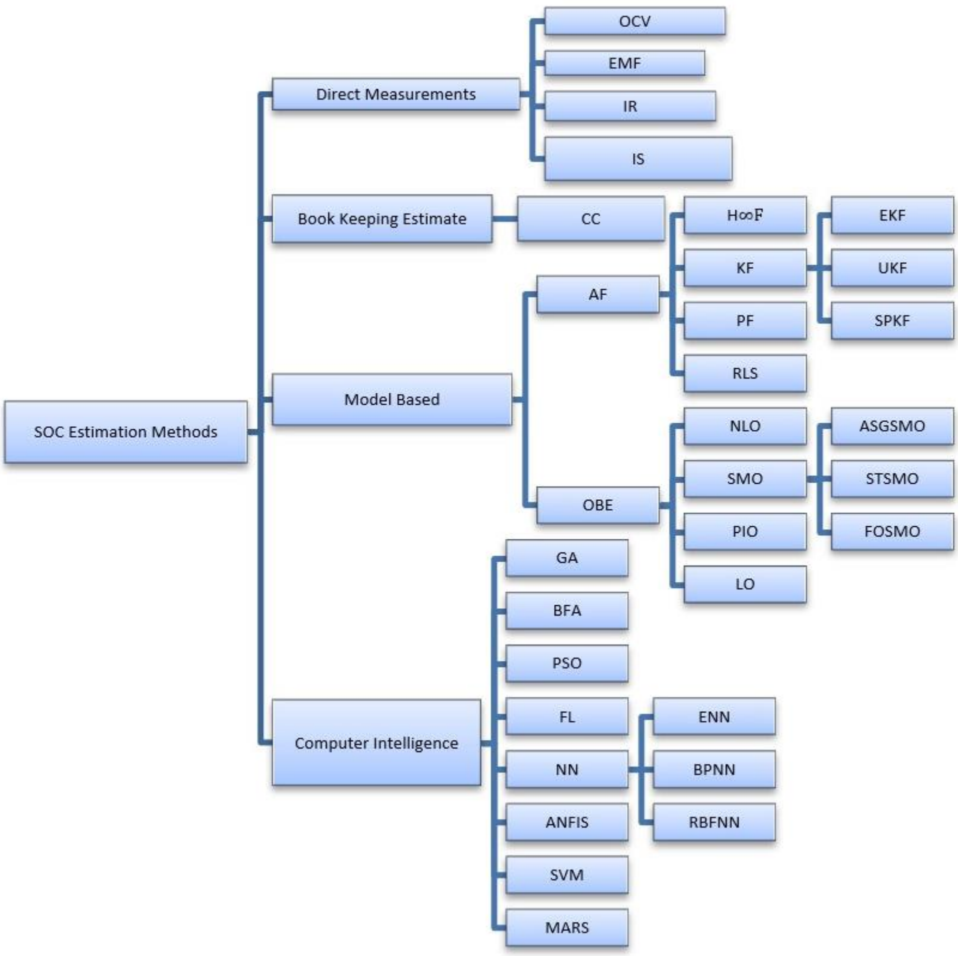

Fig. 11. Classification of SOC Estimation Methods. [28]

AF: Adaptive Filters. ANFIS: Adaptive neuro-fuzzy inference system. ASGSMO: Adaptive switching gain sliding observer. BFA: Bacterial foraging algorithm. BPNN: Back propagation neural network. CC: Coulomb Counting. EMF: Electromotive force. ENN: Elman Neural Network. EKF: Extended Kalman Filter. FL: Fuzzy Logic. FOSMO: Fractional order sliding mode observer. GA: Genetic Algorithm. H∞F: H infinity filter. IR: Internal Resistance IS: Impedance spectroscopy. KF: Kalman filter. MARS: Multivariate adaptive regression splines LO: Luenberger-

based observer. NLO: Nonlinear observer. NN: Neural network. OBE: Observer-based estimation. OCV: Open circuit voltage. PF: Particle filter. PIO: Proportional integral observer. PSO: Particle swarm optimization. RLS: Recursive least square filter. RBFNN: Radial basis function neural network. SPKF: Sigma point Kalman filter. SVM: Support vector machine. SMO: Sliding mode observer. STSMO: Super twisting sliding mode observer. UKF: Unscented Kalman filter.

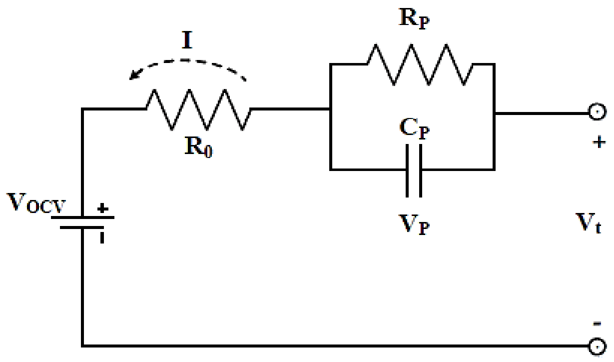

Fig. 12. Equivalent circuit of the battery

OCV is a popular strategy for measuring battery rest time, but it's not suitable for EV applications due to long resting periods and the varying relationship between SOC and OCV. Real-time OCV acquisition can resolve this issue, allowing online SOC estimates using model-based techniques. The battery's SOC is estimated using the battery equivalent circuit model and electrochemical model in standard state space[73-74]. State observers such as H∞, sliding mode, extended Kalman, adaptive Kalman, and Kalman filters are used for online estimation, affecting the accuracy of model-based techniques.

3. Methods and Data

3.1 Hardware-in-the-loop (HIL) Testing of ECU

The hardware part of the OPAL-RT system is the HIL platform, which may be used for real-time validation of the EV model and control logic. The OPAL-RT system is a simple simulation tool that enables deep correlation among electrochemical, thermal, and system-level phenomena. HIL testing is performed by omitting all of each ECU's interfaces and components that the HIL system simulates [75-77]. Equivalent electrical outputs, such as digital, analog, or variable resistance outputs, are always used to represent the sensors that are often attached [76]. The ECU's control outputs to actual or substitute loads are typically connected at the outputs, and the appropriate HIL system inputs are used to measure the ECU's control outputs [77]. Plausibly simulating sensor values at the sensor simulation HIL system's output is enabled by the controlled system's real-time competent simulation model. Rest bus simulation refers to the absence of communication on the HIL bus, as the HIL bus controller simulates it [66]. By extending these interfaces, the HIL system can be used to precisely or repeatedly generate different types of failures as needed [77-78].

3.2 HIL Test for Battery Management System (BMS)

Battery models for testing a BMS must depict the battery as a network of interconnected single cells, rather than models for simulating the car's electrical system in the traditional low-voltage range [79]. The SOC and cell voltage of a single battery cell are then modelled through a cell representation [80]. Leakage currents, dynamic behavior during abrupt load changes, and technical variations in behavior during charging and discharging are all considered [81-82]. The integration of the BMS HIL system into a vehicle simulation as a whole is the most intricate HIL simulation scenario [80]. The electrical ESS in a standard HEV or EV interacts with the gearbox, electric drives, and combustion engine, among other drivetrain parts. This study shows how thermal models and simple protection/control logic may be combined within a HIL simulation environment to assess the thermal monitoring and safety capabilities of BMS. This is a useful testbed for evaluating temperature measurement, threshold protection, and system behaviour before implementation in actual EV hardware. The "scalable battery model" lacks sufficient detail on critical aspects, including pack-level dynamics, multi-cell imbalances, aging propagation, and adaptability across different chemistries, which are essential for effective system-level modelling and simulation.

3.3 Structure of HIL System with RT-LAB

In this work, the HIL battery model's accuracy, including voltage and temperature error, is not quantitatively compared to experimental reference data, as it is derived from literature to demonstrate HIL feasibility. Future work will aim to validate the model's accuracy experimentally. The electrical and thermal models in the Hardware-in-the-Loop (HIL) environment are connected via bidirectional electro-thermal coupling.

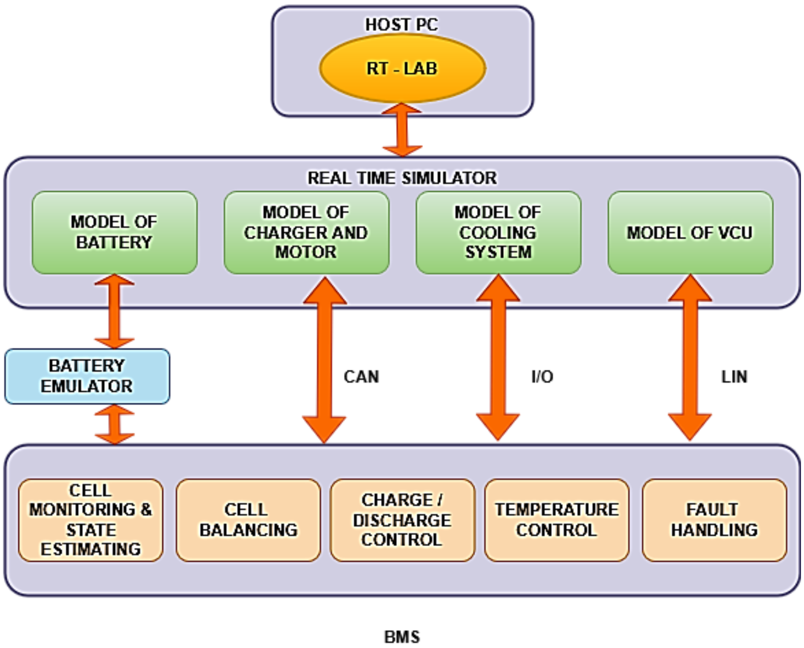

Fig. 13. Structure of HIL System

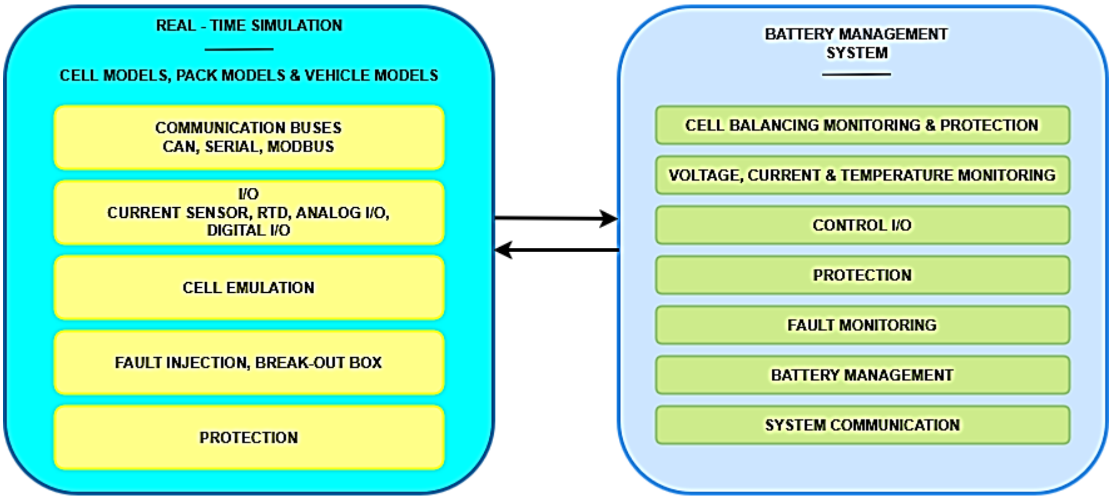

Fig. 14. Real-time HIL functional schematic

The electrical battery model calculates internal losses, like Joule heating, which the thermal model uses to determine temperature based on these heat sources. This temperature feedback is crucial for revising parameters in the electrical model and ensuring electro-thermal consistency. For SOC and SOH estimations, temperature influences the OCV-SOC relationship and internal resistance, thereby affecting estimation accuracy, though its impact varies by strategy. While sophisticated BMS can directly integrate temperature, most HIL simulations use fixed parameters, limiting robustness during temperature variations. Overall, the HIL architecture allows for parameter revision based on temperature but does not enable comprehensive temperature-aware SOC/SOH estimation, highlighting a limitation of the approach [83-88].

The HIL system, as seen in Fig. 13 below, consists of the host PC, a battery emulation, a real-time simulator, and the BMS. The host PC serves as an interface between the user and the system, running testing and simulation control applications. It provides a platform for creating simulation models and managing the simulation process using MATLAB and RT-LAB tools, respectively. We can download the simulation model to the real-time simulator and run it using RT-LAB software. A multicore CPU and an FPGA card are found in the RT-LAB HIL box, the real-time simulator that is capable of sophisticated real-time computation and I/O processing. It uses digital and analog IOs and the communication bus to interact with the BMS while computing all the models [89].

The real-time simulator manages the battery emulator, which simulates cell voltage, current balance, battery temperature, and battery defects. Other components of the BMS are connected to the real-time simulator via CAN buses and I/Os, while the monitoring and balancing unit is directly connected to the battery emulator. We can test the following BMS function items using this HIL system:

- Cell voltage monitoring
- Cell balancing
- State estimating
- Temperature control
- Fault handling
- Communication with VCU

3.4 Battery Simulation with High Electrical Requirements

A single battery cell's voltage is primarily determined by its SOC, temperature, and charge/discharge current. When the cell is not loaded, the SOC falls, and the cell voltage steadily declines.

3.4.1 Cell Model

A voltage source simulates the open-circuit voltage (VBat,0), and different impedances model the static and dynamic voltage behavior in a cell voltage model. The simplest possible substitution circuit for a car battery simulation is shown in the above picture. It comprises one RC element for double-layer capacity and charge transfer, and another RC element for the diffusion effect. The impedance spectroscopy approach is typically used to parameterize the cell voltage model. The values for the components of the replacement circuit are determined from measured spectrograms. An optimization algorithm can be used to define an automated procedure for the parameterization process. [90]. The multi-cell and pack-level SOH estimation was not covered in this study, as it focuses only on cell/module-level review and HIL validation/module level and platform feasibility. Detailed pack-level SOH modelling and scalability analysis require extensive multi-cell data, integrated thermal and aging models, and complex embedded system implementation, which are beyond the scope of this work.

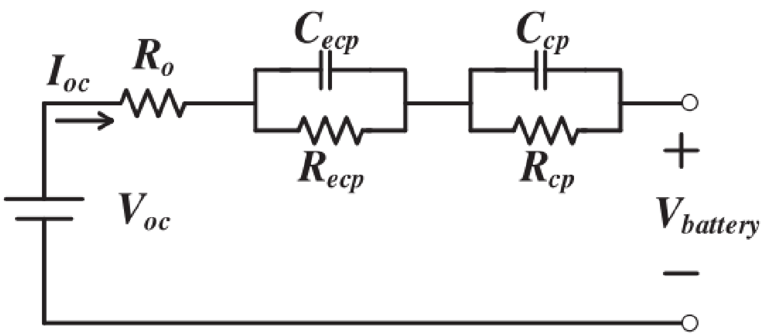

Fig. 15. Battery cell model

3.4.2 Cell Network

It is theoretically possible to create a series network of cells by joining several examples of the previously mentioned cell model. Thus, for the HIL simulation of a series cell topology, a novel strategy was adopted. Based on the assumption that a battery is composed of identical cells that consistently exhibit similar static and dynamic characteristics, the battery model is split into two sections: a reference section and a delta section.

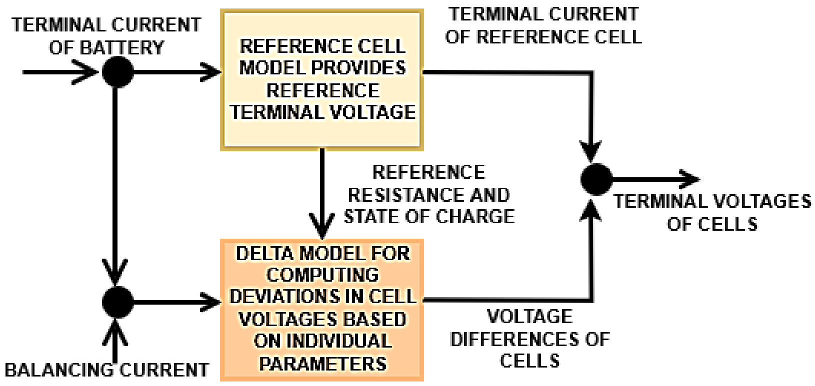

Fig. 16. Topology of the ASM multi-cell model

The delta model uses a linearized method to compute the difference between each single-cell voltage and the reference voltage. For every cell in the delta model, the capacity, starting SOC, and deviation of the internal impedances from the reference value can be provided. The new modelling strategy saves computing time on a real-time system by a factor of 12, while saving a significant amount of time in offline simulation on a PC. Fig. 17 illustrates the simulation of cell discharge using the multi-cell method compared to a model with individual cells. The cell voltage response, which is essential to the BMS's capability to balance cells, demonstrates minimal differences, particularly in the 40% to 80% SOC range.

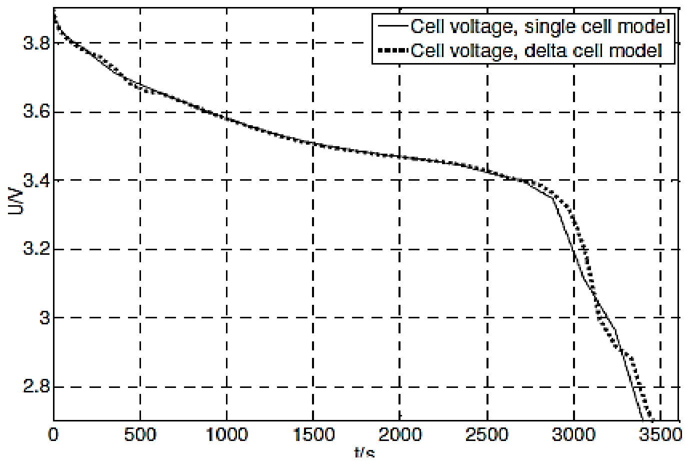

Fig. 17. Comparison of single and delta cell models

The currents in each circuit must be calculated for a parallel connection, and these currents are based on the battery's terminal voltage. For this computation, the Thevenin technique is used in the model. [91] An energy balance is used in the temperature model to determine the battery temperature.

3.4.3 Battery Model Integration

For instance, the BMS HIL system's DS1006 processor (dSpace) board can calculate the battery model in real-time when combined with models of electric drives and combustion engines, such as the ASM Engine. This enables the BMS to be tested in common hybrid drivetrain conditions. The drivetrain model can be tied to vehicle dynamics and environment simulation, such as ASM Traffic, to verify GPS and map-based control methods for the drivetrain. In the test system, these model configurations can be calculated in real-time. While accurate emulators and sensors are employed, the current work considers the electrical, thermal, aging, and control subsystems primarily independently and does not yet correlate and validate the closed-loop interactions among them; however, multi-physics correlation and pack-level closed-loop validation are specifically planned as part of the future work scope.

3.4.5 System Setup

Several interconnected cell-simulation models are required to replicate the behavior of an advanced electric vehicle battery. Battery emulators are the heart and soul of BMS HIL. It consists of the modules listed below, as shown in Figure 18. They are mentioned below-

- Communication module;
- FIU module; Cell voltage module;
- Battery temperature module;
- Balancing the current module;

A battery pack with up to 200 cells can be simulated by connecting multiple emulators in series. The battery emulator is specifically made to mimic battery cells and has 24 series-connected voltage output channels. The emulator also includes fault injection units and channels that simulate temperature. The real-time simulator, as depicted in Fig. 19, uses the CAN bus to control the battery emulator. It receives readback voltage and current data from the battery emulator, which also receives set points for cell temperatures, voltages, and FIU states.

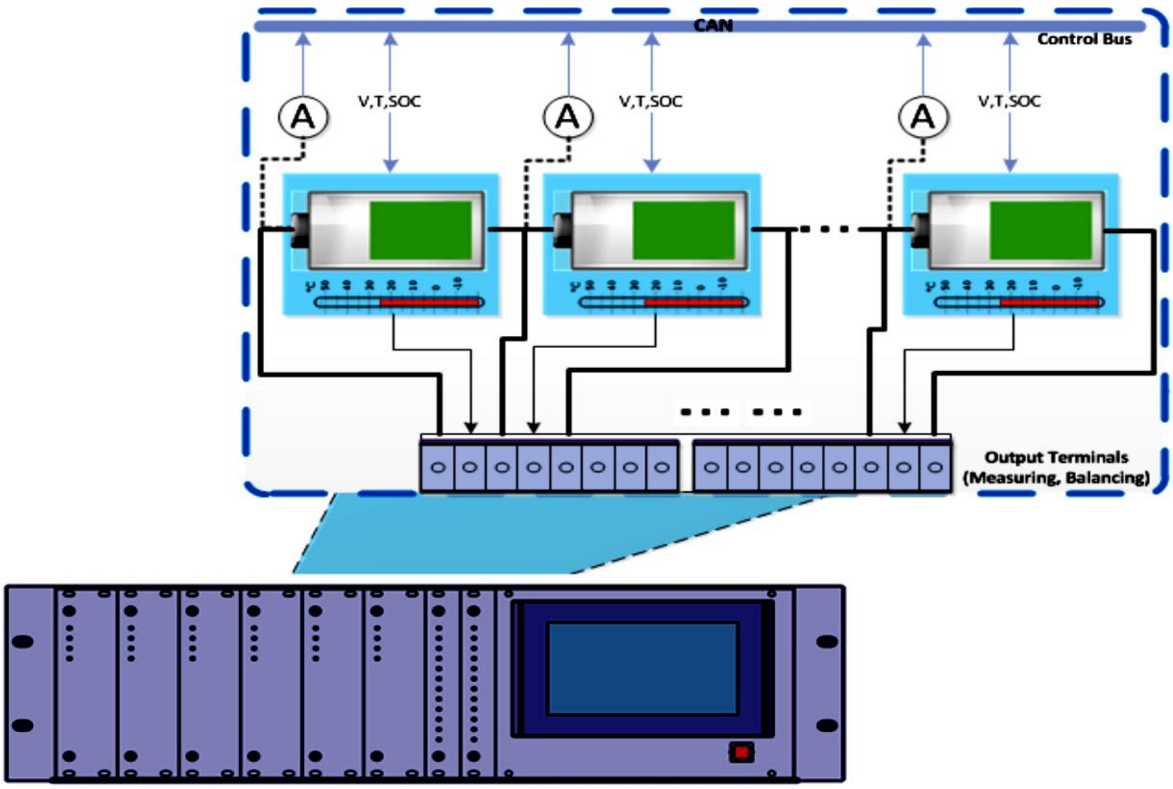

Fig. 18. Battery Emulator Structure [92]

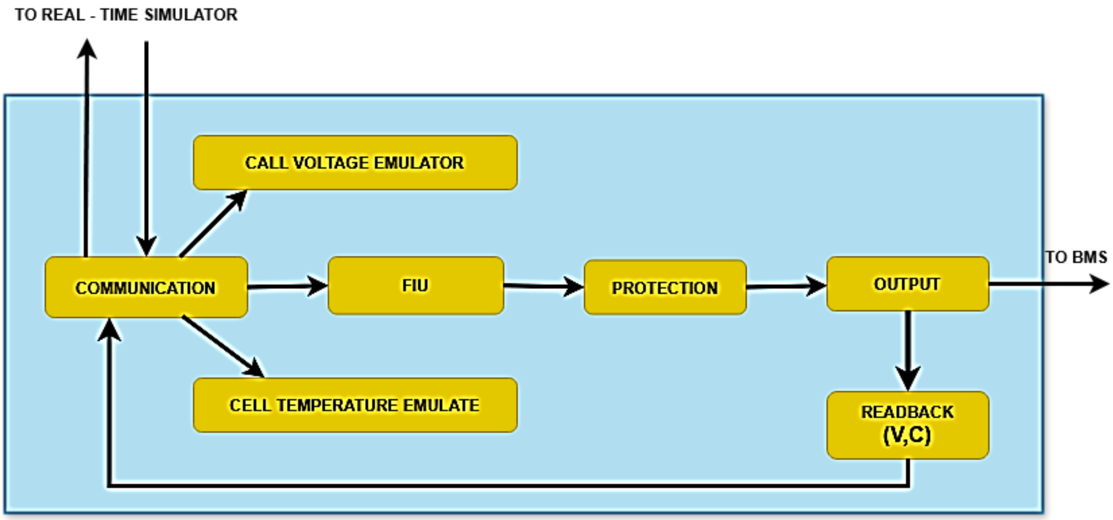

Fig. 19 Structure of the battery emulator [93-94]

3.6 Implementation

System engineering defines NFRs as specific criteria used to analyze a system's functioning, whereas FRs are defined as specific behaviors of a system's functions. Broadly speaking, NFRs specify how a specific system should function and behave, while FRs specify what a certain system should accomplish. ISO 26262 provides further information regarding functional safety requirements. Before doing HIL testing on any ECUs, it is necessary to have classified test cases. Based on these, we will execute the test and conclude.

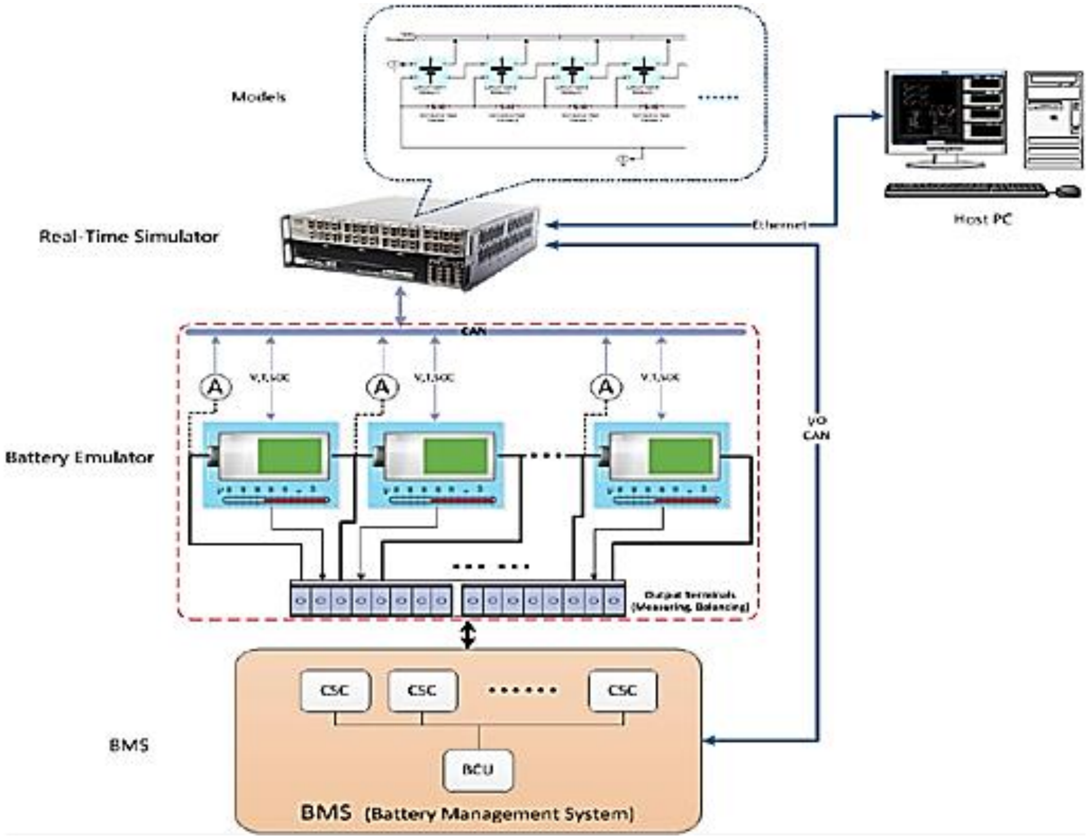

Fig. 20. Real-time Simulator OP5600 [95]

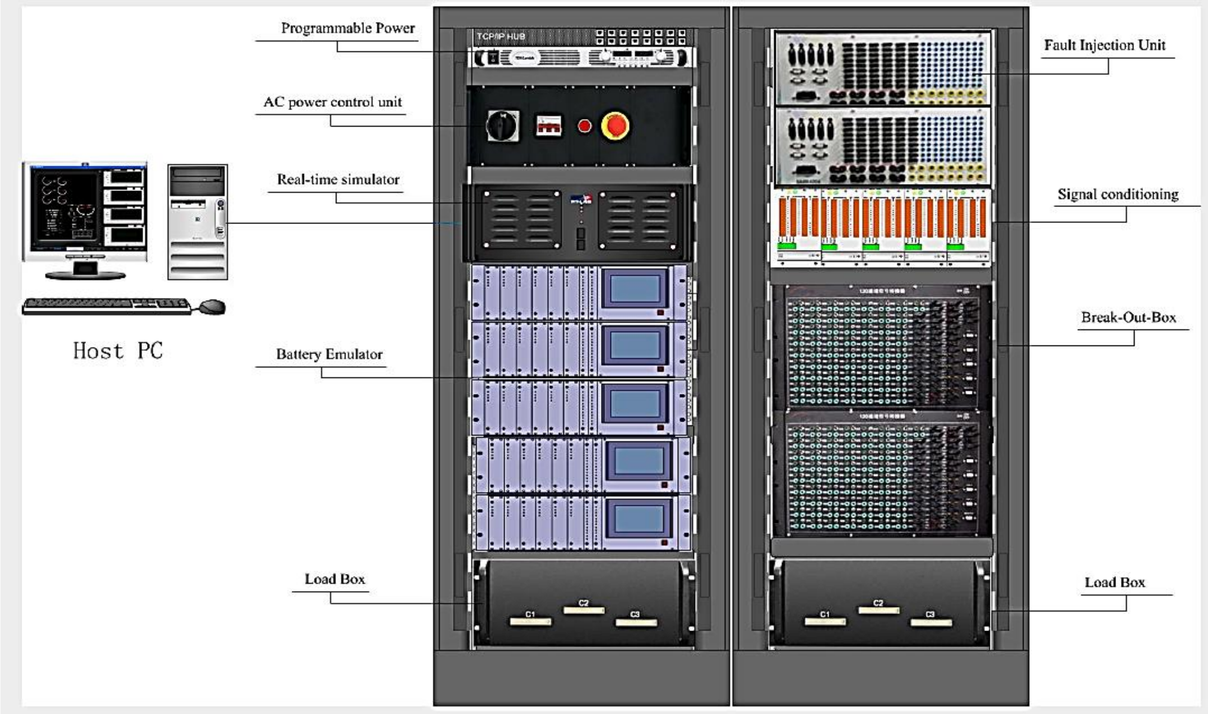

Fig. 21. HIL system hardware connection [95]

The diagram in Figure 21 displays the hardware connection for the HIL setup. Through Ethernet, bidirectional communication is established between the host PC and the real-time simulator. The real-time simulator utilizes the CAN bus to interface with the battery emulator and the I/Os, as well as the CAN bus, to communicate with the BMS central ECU. The battery emulator is directly connected to the local ECU or BMM. The BMS under test (DUT) comprises multiple BMMs and a central ECU. BMMs are modularized components that track temperature, current, and battery cell voltage. The BMMs are managed by the central ECU via the real-time CAN bus. Furthermore, the CECU manages temperature, fault handling, charge/discharge control, and communication with the VCU in addition to completing SOC estimates.

The operating conditions are specified before testing begins, such as the charging or city driving processes that generate various charging sources or battery-draining loads. The IO, CAN, and battery emulator outputs are updated in real-time, based on the operational state. The BMS examines every state and adapts to any modifications. The real-time simulator receives the BMS's data and readback. After that, they are regularly updated and contrasted with the actual values. To wrap up the test cases, the test results are achieved after completing the necessary iterations. Multi-cell and pack-level SOH estimation was not covered, as the current study is only a review and HIL validation, with its scope primarily on cell/module-level ideas and platform feasibility. Comprehensive pack-level SOH modeling, estimation, and scalability studies are extensive and require large multi-cell data, integrated thermal and aging models, and large-scale embedded system implementation, which are outside the current study's scope. These are proposed for future work, including pack-level SOH fusion, weak-cell identification, imbalance-aware aging modeling, and scalable, real-time implementation for EV-grade BMS.

Table 2. Test cases suggested for testing a BMS for its Functional Requirements (FRs) and Non-Functional Requirements (NFRs) [92-103]

No	Test Case	Description	End-of-test Criteria
1	Idle or stand-by	System settings are controlled. The fault criteria are defined in the BMS. The next functions are examined in steady-state: data management, monitoring, hazard detection, and hazard response.	All functions tested in steady state

2	Temperature, Current, and Voltage sensing	All sensors are calibrated, if possible. Then, full-range accuracy tests are performed while keeping the BMS under various conditions, e.g., in a temperature chamber.	All conditions tested
3	Dynamic discharge	By employing a real dynamic discharge profile of an EV, the pack is discharged to room temperature.	BMS stops the discharge to avoid over-discharge
4	Over-temperature during discharge	Applying a real dynamic discharge profile of an EV, the pack is discharged at high temperature.	The pack reaches maximum temperature, and the BMS stops the discharge.
5	Overvoltage during regenerative braking	Employing a real dynamic discharge profile of an EV, the pack is completely discharged when a very high regenerative current is encountered.	The BMS interrupts the regenerative charging current.
6	Short Circuit	Shorts at different places in the pack. Case I: internal or external short close to cell tabs. Case II: external short through fuses or shunt resistor, Case III: External short through fuse and switch box (relays or fuses)	The short circuit current is zero.
7	CCCV Charge	Conventional CCCV charge with active/passive balancing.	End of charge
8	Charge test at low temperatures	The charge is allowed, but the pack temperature is below the charging limit. Temperature rises gradually due to the heating system.	Pack temperatures over the threshold, and charging starts
9	Diagnosis	Case I: Simulated SOC vs. BMS-approximated SOC throughout a real dynamic discharge profile from an EV. Case n: New cases based on the BMS diagnosis features.	End of charge and discharge
10	Isolation Monitor	Single isolation failure on the positive/negative terminal of a floating voltage pack	Isolation fault detected
11	Global power consumption	Case I: Full discharge, taking into account a dynamic discharge profile from an EV, and subsequent CCCV charge, Case II: Stand-by test for a period of time.	BMS power consumption is measured under all conditions

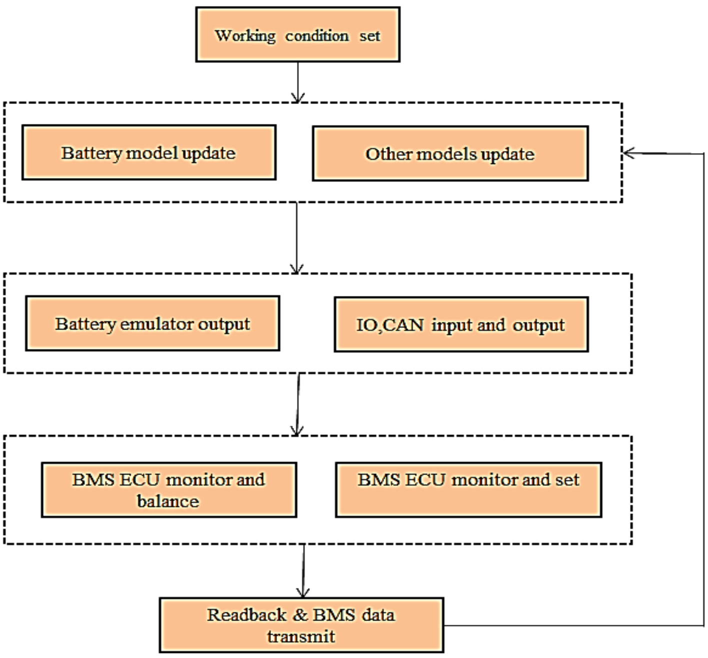

Fig. 22. Working process of BMS testing

4. Results and Discussion

This section displays the experimental findings of the BMS's communication with the system-level HIL-simulated battery. Regarding test case 2 (Table I), Figure 23 provides details about the calibration of the pack current sensor. Calibrating the sensor is one of the first steps in evaluating the accuracy of a BMS product. However, for two arbitrary sensing lines in the BMS, the figure shows exemplary data on the accuracy of cell voltage sensors at various temperatures and voltage levels.

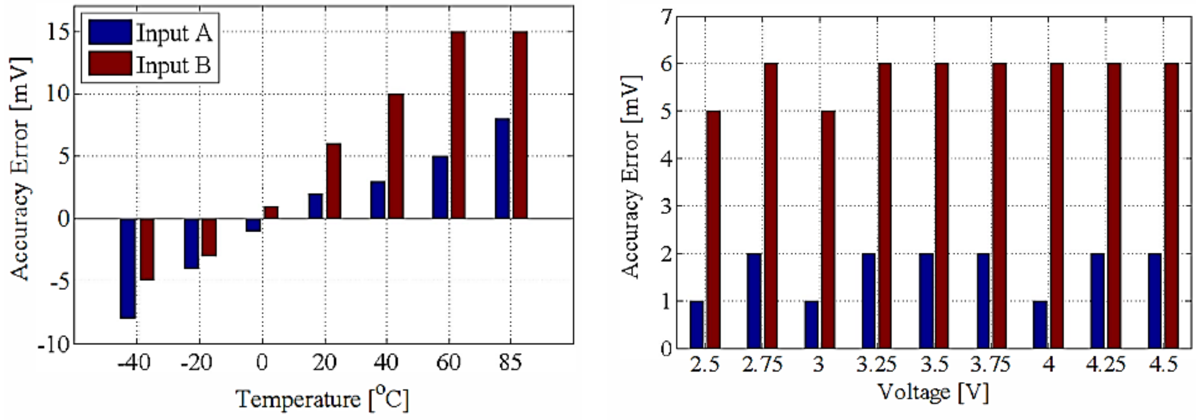

Fig. 23. Test case 2 revealing cell voltage sensing accuracy, (a) Cell voltage measurement accuracy at various temperatures and (b) a) Cell voltage measurement accuracy at various voltages [95]

Figure 24 illustrates the plotted results of an overvoltage that occurred during regenerative braking, corresponding to test case 5 (Table I). A robust regeneration current at high SOC levels may cause an overvoltage in specific battery cells. To stop the excessive inrush current, the BMS recognizes the hazard and opens the switch box's relays. It is possible to design the BMS to close the relays and resume discharge mode operation after a predetermined amount of time.

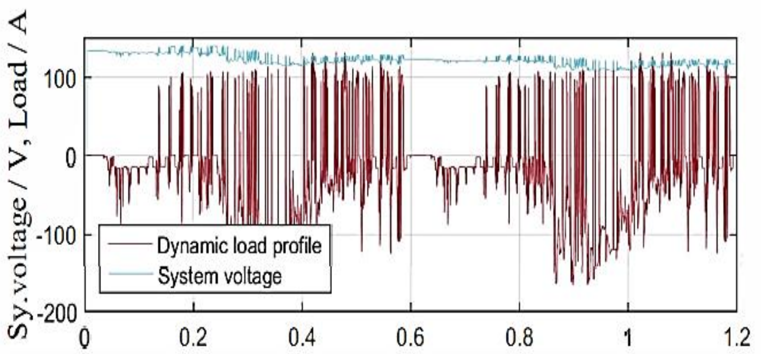

(a)

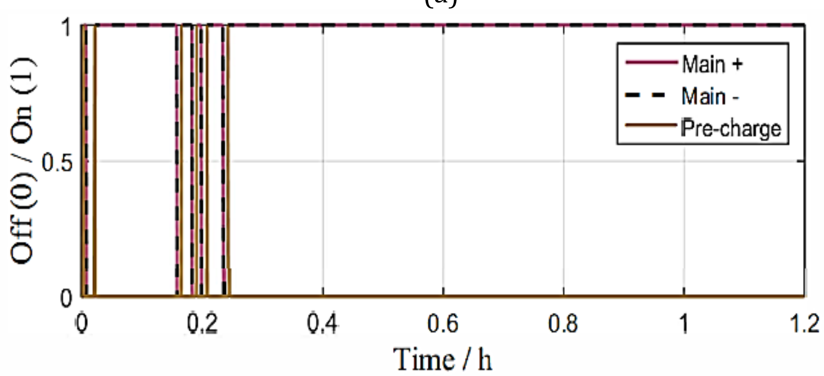

(b)

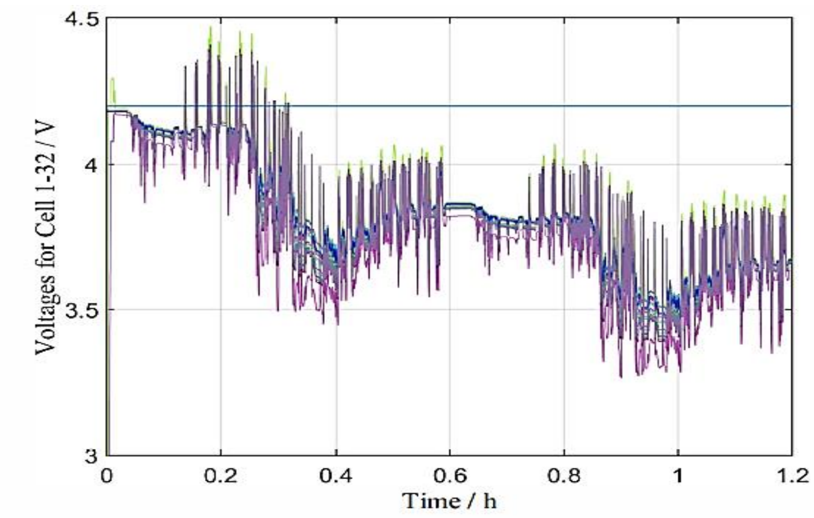

(c)

Fig. 24. Test case 5: Overvoltage during regenerative braking (a) Pack voltage and pack current in time (b) Switch box contactor logic and (c) Cell voltages in time and max. voltage threshold [95]

Test case 4 (Table I), which involves over-temperature during discharge, is illustrated in Fig. 25. For this test, predetermined high starting temperatures and constrained cooling capacities are utilized. As a result, during discharge, the cells in the pack overheat. Once more, the BMS recognizes the danger and stops the discharge by opening the relays in the switch box. The BMS can be set to shut the relays and resume operating in discharge mode after a predetermined amount of time once the issue has been resolved.

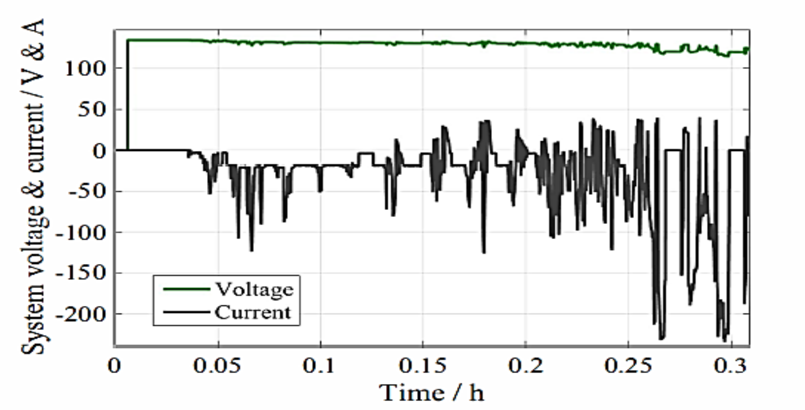

(a)

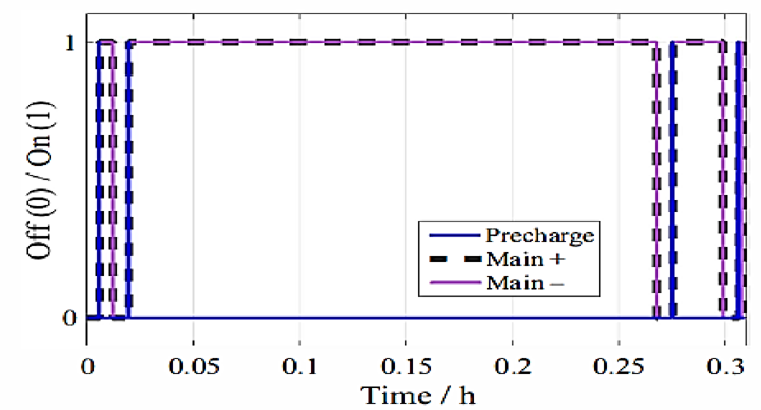

(b)

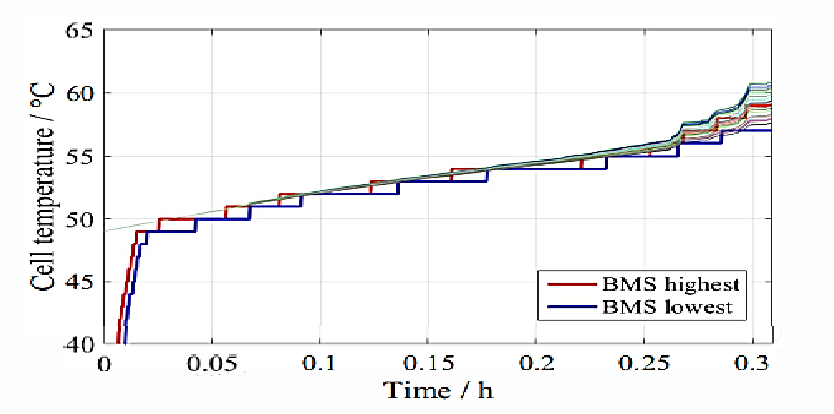

(c)

Fig. 25. Test case 4: over temperature during discharge (a) Pack voltage and pack current in time (b) Switch box contactor logic and (c) Experimental vs BMS measured cell temperature [95]

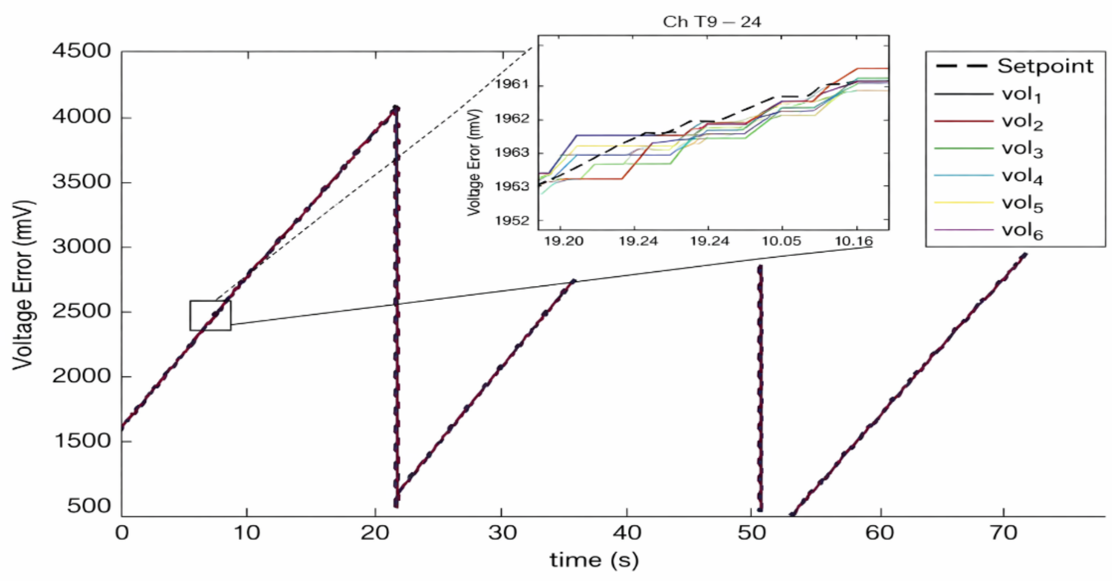

Fig. 26. Output accuracy of battery emulator [80]

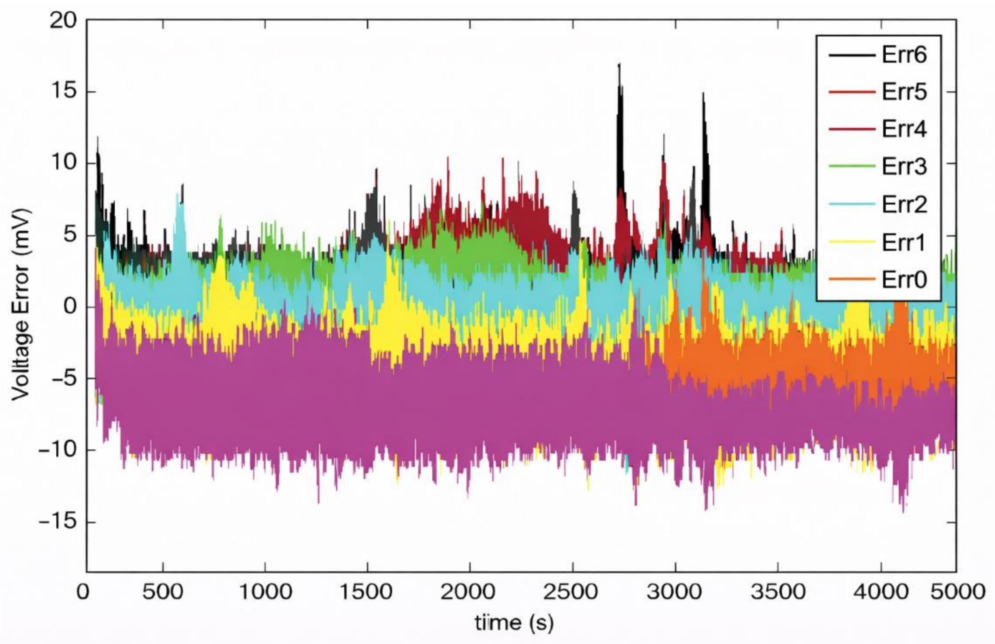

Fig. 27. Voltage monitoring error of BMS [80]

The figure presents the system behavior during operation in three subplots. Figure (a) shows the system voltage and current over time, where the voltage remains relatively stable while the current exhibits fluctuations and negative peaks due to load variations. Figure (b) illustrates the switching states of the pre-charge, main positive, and main negative contactors, indicating their on/off operation during the process. Figure (c) shows the cell temperature evolution, where both the highest and lowest cell temperatures gradually increase from about 40 °C to around 60 °C, demonstrating the thermal response of the battery pack during operation.

Figure 26 shows the voltage error response of six voltage channels (vol_1–vol_6) compared with a reference setpoint over 0–70 s. The setpoint follows a repeating ramp pattern, and all channels closely track it with minimal deviation. The inset (19.20–19.24 s) highlights millivolt-level tracking accuracy, indicating stable and high-performance voltage control or estimation. The output of the battery emulator is compared with the set point in Fig. 26. As shown, the outputs of all six channels provide very accurate results, with errors of less than ±2 mV. This indicates that the battery emulator's readback and output are reliable and represent the actual value.

Figure 27 shows the voltage error variation of six signals (Err_1–Err_6) over 0–5000 s. Most errors remain within −10 mV to +10 mV, indicating stable and accurate voltage estimation. Occasional peaks around 2500–3200 s appear due to transient disturbances. The voltage-monitoring error of the BMMs (LECU) under test is shown in Fig. 27, along with a comparison to the battery emulator's readback value, which remains approximately 10 mV.

5. Conclusions

The work focuses on foundational modelling and framework development for estimating SOC, SOH, and SOP, rather than introducing new estimation algorithms. Key contributions include the establishment of accurate battery behavior models essential for any estimation approach, and a validated simulation framework for performance evaluation under realistic conditions. It also identifies practical limitations and sensitivities of SOC/SOH/SOP indicators to measurement noise and operating conditions, informing future estimator designs. Furthermore, it specifies the necessary inputs and metrics for applying advanced methods, such as EKF/UKF and neural networks, in future development, thereby creating a reliable baseline for subsequent SOC, SOH, and SOP estimation algorithms. It summarizes and discusses current approaches and their validation in a real-time HIL environment using OPAL-RT/RT-LAB, rather than creating new algorithms for SOC/SOH estimation, thermal management, or AI-based diagnosis. The manuscript offers an implementation-focused perspective on BMS, linking recent algorithms and architectures to HIL validation. It highlights new insights into testability, real-time capability, and prototyping feasibility, addressing the gap between simulation-based research and practical EV BMS development not previously emphasized in reviews from 2019 to 2024. This study contrasts several important BMS technology features with the benefits of Li-ion batteries and other ESS. Its long life, high energy and power density, and nominal voltage make the Li-ion battery a highly recommended choice for electric vehicle applications. However, lowering capital costs remains a significant obstacle. This review also thoroughly categorized the best charging topologies, thermal management, and SOH and SOC estimations for Li-ion batteries. As they become available in the literature, several algorithms and technologies have been presented. Upcoming difficulties have also been highlighted. Consequently, to address these challenging problems, it is necessary to establish confidence intervals for the methods and algorithms under consideration. Afterward, RT-LAB is used to verify the BMS by interfacing with the HIL system. The HIL setup can model up to N cells/modules in real time on the target hardware, adhering to a simulation time step of $\Delta t = 1$ ms. Beyond this limit, real-time constraints are not satisfied. The minimum stable real-time step for the model is $\Delta t\_min = 0.5$ ms.

A general discussion of testing definitions and aims was presented, emphasizing the fact that there is a wide range of opinions. Various test cases have been suggested to verify the dependability of the system. Since it is not always possible to verify every scenario that theoretical techniques provide, some essential elements of the system are often preferred as theoretical frameworks. On a commercial HIL simulator, an effective approach to generating SW and testing techniques for BMS at the system level was demonstrated. Extensive experimental data were collected after comprehensive test cases were suggested. Different scenarios were shown to illustrate the interactions between the real-time simulator and BMS. The conclusion lacks explicit identification of technical limitations, applicability scope, or future research directions for a comprehensive BMS framework, which are anticipated to be addressed in future work. The conclusion lacks explicit identification of technical limitations, applicability scope, or future research directions for a comprehensive BMS framework, which are anticipated to be addressed in future work. The research does not include a validation or benchmarking framework, focusing instead on reviewing existing methodologies and showcasing the feasibility of HIL simulation. It lacks systematic performance comparisons under EV drive cycles, benchmarking against reference models, validation with experimental baselines, and evaluation using recognized performance metrics.

5.1 Limitations of the Method

The manuscript offers an overview of BMS research and HIL platform significance for validation but inadequately discusses practical implementation methods for real-time embedded systems. It fails to address essential aspects like microcontroller computational complexity, real-time capabilities of SOC/SOH estimation algorithms, stability under varying EV loads, and sensor noise considerations. Key elements such as sampling rate, memory and power usage, task scheduling, communication delays, and robustness to hardware issues are also overlooked, raising concerns about the transition from simulation to real-time applications in vehicles and the technology's readiness.

- Model Accuracy: The real-time battery model may not capture all complex electrochemical phenomena and non-linear behaviors, particularly under extreme operating conditions or advanced aging scenarios.
- Hardware Constraints: Opal-RT platform computational limitations may restrict model complexity and resolution, while processing delays could introduce timing inaccuracies not present in actual battery systems.
- Limited Validation Scope: Testing appears focused on standard operating conditions, potentially excluding extreme scenarios like thermal runaway, and may not encompass the full range of Li-ion chemistries or environmental conditions.
- Scalability Uncertainty: While described as scalable, real-time performance with large EV battery packs (hundreds of cells) remains unclear, with computational requirements potentially increasing exponentially.
- BMS Function Coverage: The study may not address all advanced BMS functions, such as predictive maintenance, adaptive algorithms, or cybersecurity features, limiting comprehensive system validation.
- Experimental Data Limitations: Model characterization may be restricted to specific battery types and conditions, with measurement uncertainties potentially affecting validation accuracy.
- Industry Application Gap: Results may not translate directly to all commercial BMS platforms due to hardware/software differences, and cost-benefit analysis versus traditional testing is not addressed.
- Technology Evolution: Rapid battery technology advancement may quickly outdate models, while emerging technologies like solid-state batteries may require entirely different approaches.
- Benchmarking Deficiency: Limited comparison with other HIL platforms or real-world testing results makes it difficult to quantify simulation accuracy and effectiveness.
- Long-term Validation: Insufficient long-term degradation data may affect the accuracy of state-of-health and remaining useful life estimations critical for BMS performance.
- Advanced Technology: AI can be implemented to increase the efficiency of the BMS
- Maintenance: Improper maintenance of the BMS may degrade the efficiency of the usage
- Space Requirement: The requirement for space can be optimized to increase its efficiency

5.2 Future Prospectives

Some prospects of Li-ion battery technologies are mentioned below.

- There should be some efficiency improvements, Depth of Discharge (DOD), and energy density of Li-ion batteries. The main concern is the increase in capital cost.
- The RC-structured ECM estimation could be more precise using some complex mathematical models.
- Most of the research of the recent era has been conducted in a lab environment. But the actual scenario could differ if we run the tests under different environmental conditions, such as snowy, humid, hot, or cold.
- Errors in SOC or SOH estimations could be lessened with further research.
- The different algorithms used in battery models could be more optimized.
- Most of the time, current sensors are corrupted by measurement noise.
- Real-time SOH estimation is a big problem.

The current study lacks integration of advanced methods and does not evaluate their feasibility for embedded systems. It fails to address critical questions regarding data requirements, training/validation processes, generalization for various cells and temperatures, computational and memory demands on ECUs, real-time inference delays, interpretability, and safety certification. Consequently, the manuscript primarily serves as a survey or HIL demonstration, not demonstrating how AI or hybrid BMS approaches can be embedded and validated for electric vehicle-grade implementation.

While the proposed HIL development methodology can be applied to commercial BMS hardware, its suitability for production-grade automotive systems remains unproven. It lacks explicit consideration of automotive communication protocols and various safety and validation standards, including ISO 26262, ASPICE, ISO 12405, and SAE J2464. Consequently, the framework is perceived as more research-oriented than validated for production use.

6. Appendix

V-Model Development of BMS: A Case Study

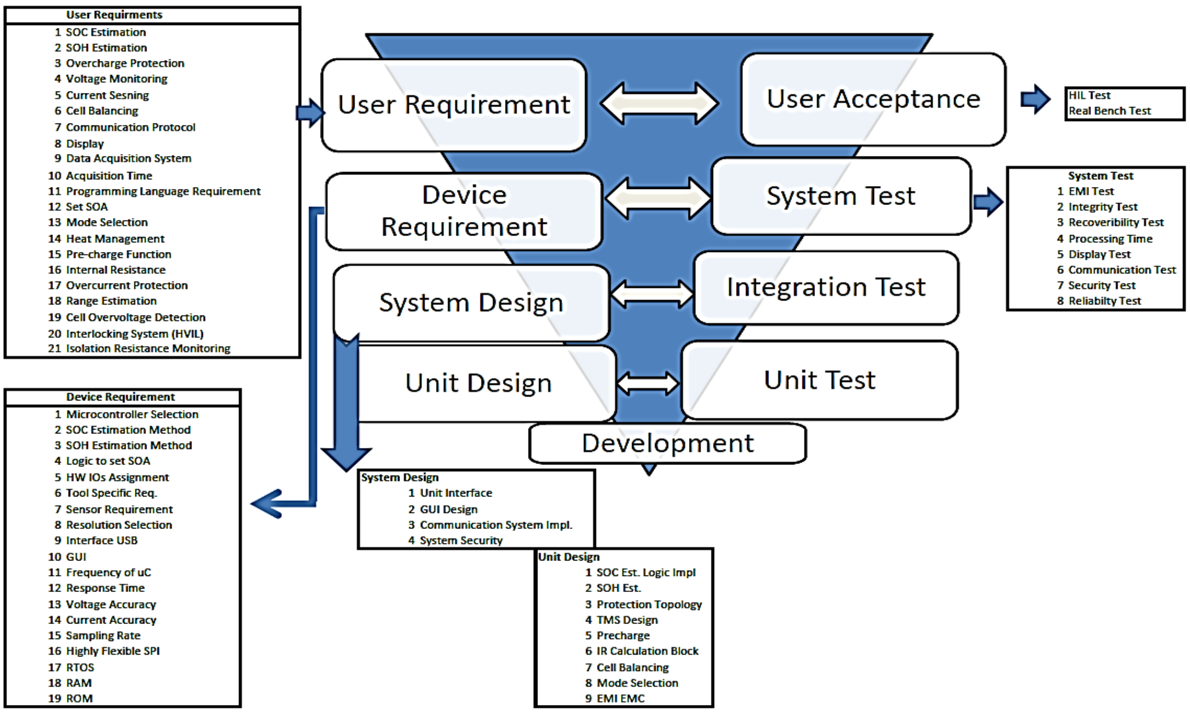

BMS Generic HIL Test Cases

Sl. No.	Test Case	Description of Test	Criteria for Test Completion
1	Wake Up	Wake-up signal is sent to BMS, and receives confirmation from BMS to HIL	If firmly get a Rx signal from BMS
2	Check Sum	Every Signal should come from the BMS to the host PC via HIL communication buses.	Every signal code should be floated.
3	Idle or Standby	Making the system ready to use, but not connecting any load. The fault criteria are set in the BMS.	Readiness time was within the time limit, and no faults were detected.
4	Isolation Monitoring	Isolation resistance between the chassis and the battery pack should be within the limit. An external sliding resistor could be connected to create a manual situation.	If any leakage happens, BMS should send signals to VCU and take proper action according to ISO26262 (ASIL-C)
5	Battery CAN_H & CAN_L signals	CAN High and CAN Low should come from all BMMs to the BMS	Rx and Tx are coming properly.
6	V CAN_H & V CAN_L	Vehicle CAN communication between VCU and BMS	Rx and Tx are coming properly.
7	Cell Balancing	Active and passive balancing should be correct, and the time taken for balancing should match the predefined value.	Balancing is happening correctly.
8	Pre-charge	To charge the battery, the OCV of the battery should be equal to the charger's output voltage to avoid sparks and hazards. To achieve this, a capacitor, a resistor, and a relay-based circuit are employed. Testing the recharge operation.	Pre-charge circuitry is functioning properly, ensuring the safe operation of the relay.
9	HVIL Check	Due to an interruption in the current flow through the High Voltage Interlocking Loop, the vehicle should stop. Moreover, BMS should disconnect the battery from the vehicle system. (ASIL C)	Manually created a faulty situation with the help of an NC switch, and the BMS stops operation.
10	Temperature Sensing	A 12V temperature signal in all the BMMs from the temperature sensors, thus in the BMS via CAN	If Rx signals are coming into the BMS
Sl. No.	Test Case	Description of Test	Criteria for Test Completion
11	Temperature Cut Off	Based on temperature rises and dips, the BMS should take action by sending a proper signal to the Coolant tank. If the maximum temperature is reached, the BMS should disconnect the battery.	Proper coolant rate as predefined calculated rate and stop battery in overtemperature
12	Current Sensing	Current-sensing signals from all current sensors to the BMS.	Getting an accurate sensing signal.
13	Current Cut Off	Required charging and discharging currents should be measured. Beyond the specified limits for minimum and maximum currents, the BMS should take appropriate action.	If the maximum current is reached, it should stop draining the battery.
14	Voltage Sensing	Voltage-sensing signals from each cell should come to the BMS via the BMMs from the voltage sensors.	Getting all signal codes in the HIL host PC.
15	Voltage Cut Off	Overvoltage and undervoltage situations should be addressed by the BMS through appropriate action.	Successfully enabling the cut-off circuitry operation.
16	SOC Estimation	Are the estimated SOC and emulated SOC the same or not	If they are equal
17	CCCV Charge	Conventional CCCV charging happens with successful active/passive balancing.	End of the charge
18	Under and Overcharge	SOC levels typically range from 20% to 80%. The SOC limits for both cases should be within the same range.	Successfully enabled the protection circuitry and disengaged the battery for both cases.
19	Coolant Flow	Calibrated temperature rise Vs. Coolant flow rate should be maintained. Checking predefined flow rate Vs. temperature curve.	The curve is true for every operating point.
20	Handshaking with a charger	Before charging starts, proper handshaking should occur between the BMS and the CCU (Charger Control Unit) over a dedicated CAN channel.	Handshake successful and reached the ready-to-charge state.

21	Regenerative Braking	In the case of regenerative braking, the BMS should act accordingly.	Action taken is successful.
22	Data Acquisition	All data is stored in the BMS.	Data can be extracted and matched with predefined set points.
23	Diagnosis	Checking whether any fault happens or not through the OBD connector and the handle given in the BMS. Diagnosis happens according to ISO14229.	Successfully diagnosed.

References

[1] Bang H, Dave A, Tzortzoglou FN, Wang S, Malikopoulos AA. On Mobility Equity and the Promise of Emerging Transportation Systems. IEEE Trans Intell Transp Syst. 2025;26(7):10623-10637. https://doi.org/10.1109/TITS.2025.3548885

[2] Saeed A, Alawi A, Sharqawy MH, Al Janaideh M. Advancements in Temperature-Sensing Technologies for Lithium-Ion Batteries in Electric Vehicle Thermal Management Systems: A Comprehensive Review. IEEE Sens J. 2025;25(23):42442-42461. https://doi.org/10.1109/JSEN.2025.3616085

[3] Hu B, Ioannou PA. Survey of Electric Truck Technologies and Infrastructure Support. IEEE Intell Transp Syst Mag. 2025;17(5):72-90. https://doi.org/10.1109/MITS.2025.3573644

[4] Yadav IC, Bajpai RS, Gupta S, et al. Hybrid fuzzy-MPC based multi-objective control strategy for fast charging of electric vehicles with advanced battery thermal management and renewable grid support. Sci Rep. 2025;15:42342. https://doi.org/10.1038/s41598-025-26279-4

[5] Chen J, Zhang X, Zhou Y, Chen G, Zhai Q, Cao Y. Optimal Joint Scheduling of Distribution Network and Electric Vehicle Tracks Considering Actual Carbon Emission Responsibility. IEEE Trans Transp Electrif. 2025;11(5):11075-11087. https://doi.org/10.1109/TTE.2025.3570747

[6] Roy S, Majumder S, De K, Ahmad F, Boumaiza A. Electric vehicles and environmental sustainability: Integrating material, energy, and emission flows in a system-level LCA. Sustain Dev. 2026;34(1):851-872. https://doi.org/10.1002/sd.70269

[7] Taylor W, Krithivasan G, Nelson JJ. System safety and ISO 26262 compliance for automotive lithium-ion batteries. In: Proceedings of the 2012 IEEE Symposium on Product Compliance Engineering; 2012 Nov 5-7; Portland, OR, USA. p. 1-6. https://doi.org/10.1109/ISPCE.2012.6398297

[8] Hussein HH, Batarseh I. A review of charging algorithms for nickel and lithium battery chargers. IEEE Trans Veh Technol. 2011;60:830-838. https://doi.org/10.1109/TVT.2011.2106527

[9] Dey S, Mohon S, Pisu P, Ayalew B. Sensor fault detection, isolation, and estimation in lithium-ion batteries. IEEE Trans Control Syst Technol. 2016;24:2141-2149. https://doi.org/10.1109/TCST.2016.2538200

[10] Kang Y, Duan B, Zhou Z, Shang Y, Zhang C. Online multi-fault detection and diagnosis for battery packs in electric vehicles. Appl Energy. 2020;259:114170. https://doi.org/10.1016/j.apenergy.2019.114170

[11] Wang Z, Hong J, Liu P, Zhang L. Voltage fault diagnosis and prognosis of battery systems based on entropy and Z-score for electric vehicles. Appl Energy. 2017;196:289-302. https://doi.org/10.1016/j.apenergy.2016.12.143

[12] Dutta S, Majumder S, De K, et al. Electric vehicle battery recycling for sustainability: environmental and water benefits. Clean Techn Environ Policy. 2026;28:28. https://doi.org/10.1007/s10098-025-03402-7

[13] Padmaraj O, Satyanarayana N, Suthanthiraraj SA, Venkateswaran C. Issues and challenges of rechargeable lithium batteries. Rechargeable Lithium-Ion Batteries. 2020:38-98. https://doi.org/10.1201/9781351052702-2

[14] Sethi P, Pathak M, Sharma PK, Saxena V, Dixit SK. A comprehensive research paper on lithium-ion batteries: Advances and challenges of battery management systems (BMS). Vol 1, Issue 4. 2025.

[15] Nekahi A, Madikere Raghunatha Reddy AK, Li X, et al. Rechargeable Batteries for the Electrification of Society: Past, Present, and Future. Electrochem Energy Rev. 2025;8:1. https://doi.org/10.1007/s41918-024-00235-8

[16] Yap JW, Lee M, El Idrissi F, Ramesh P, Yoon DY, Kang CY, et al. Unveiling real-world aging mechanisms of lithium-ion batteries in electric vehicles. J Energy Storage. 2025;130:117420. https://doi.org/10.1016/j.est.2025.117420

[17] Madani SS, Shabeer Y, Allard F, Fowler M, Ziebert C, Wang Z, et al. A Comprehensive Review on Lithium-Ion Battery Lifetime Prediction and Aging Mechanism Analysis. Batteries. 2025;11:127. https://doi.org/10.3390/batteries11040127

[18] Toprak MM, Kok C, Mert SO. Analysis of various flow field designs for PEM fuel cells used in vehicular systems through 3D modelling. Res Eng Struct Mater. 2022;8(1):179-203. http://dx.doi.org/10.17515/resm2021.328en0805

[19] Lozano Ruiz P, Damianakis N, Ram Chandra Mouli G. Physics-Based and Data-Driven Modeling of Degradation Mechanisms for Lithium-Ion Batteries-A Review. IEEE Access. 2025;13:21164-21189. https://doi.org/10.1109/ACCESS.2025.3535918

[20] Yardimci AI, Acikbas Y, Capan R. SEM images of carbon nanotubes (CNTs): Effect of voltage and spot size on image resolutions. Res Des. 2024;1(1):43-51. https://doi.org/10.17515/rede2024.004en1116rs
[21] Ma X, Meng Z, Bellonia MV, et al. The evolution of lithium-ion battery recycling. Nat Rev Clean Technol. 2025;1:75-94. https://doi.org/10.1038/s44359-024-00010-4
[22] Meng W. Recycling technologies of spent lithium-ion batteries and future directions: A review. Trans Nonferrous Met Soc China. 2025;35(1):271-295. https://doi.org/10.1016/S1003-6326(24)66679-3
[23] Coskun T, Çetkin E. Vascularized mini cooling channels to achieve temperature uniformity: Battery thermal management and electronic cooling. Res Eng Struct Mater. 2023;9(3):675-685. http://dx.doi.org/10.17515/resm2022.585ma1121
[24] Ralon P, Taylor M, Ilas A, Diaz-Bone H, Kairies K. Electricity storage and renewables: Costs and markets to 2030. Abu Dhabi: International Renewable Energy Agency; 2017.
[25] Westbrook MH. The electric car: Development and future of battery, hybrid and fuel-cell cars. Stevenage: IET; 2001. https://doi.org/10.1049/PBPO038E
[26] Hu X, Zou C, Zhang C, Li Y. Technological developments in batteries: A survey of principal roles, types, and management needs. IEEE Power Energy Mag. 2017;15:20-31. https://doi.org/10.1109/MPE.2017.2708812
[27] Ali MU, Zafar A, Nengroo SH, Hussain S, Alvi MJ, Kim HJ. Review towards a Smarter Battery Management System for Electric Vehicle Applications: A Critical Review of Lithium-ion Battery State of Charge Estimation. Energies. 2019;12:446. https://doi.org/10.3390/en12030446
[28] Liu K, Li K, Peng Q, Zhang C. A brief review on key technologies in the battery management system of electric vehicles. Springer; 2018. p. 1-18. https://doi.org/10.1007/s11465-018-0516-8
[29] Ali MU, Zafar A, Nengroo SH, Hussain S, Alvi MJ, Kim HJ. Review towards a smarter Battery Management System for Electric Vehicle Applications: A Critical Review of Lithium-ion Battery State of Charge Estimation. Energies. 2019;12:446. https://doi.org/10.3390/en12030446
[30] Xiong R, Tian J, Mu H, Wang C. A systematic model-based degradation behaviour recognition and health monitoring method for lithium-ion batteries. Appl Energy. 2017;207:372-383. https://doi.org/10.1016/j.apenergy.2017.05.124
[31] Lam L, Bauer P. Practical capacity fading model for Li-ion battery cells in electric vehicles. IEEE Trans Power Electron. 2013;28:5910-5918. https://doi.org/10.1109/TPEL.2012.2235083
[32] Eddahech A, Briat O, Bertrand N, Delétage JY, Vinassa JM. Behavior and state-of-health monitoring of Li-ion batteries using impedance spectroscopy and recurrent neural networks. Int J Electr Power Energy Syst. 2012;42:487-494. https://doi.org/10.1016/j.ijepes.2012.04.050
[33] Borahel RDS, Telli GD, Bolzoni AA, Isoldi LA, dos Santos ED, Luiz Rocha AO. Numerical analysis of the impact of PCM reservoir width on lithium-ion battery cooling: A constructal design study. Res Eng Struct Mater. 2025;11(5):2421-2435. https://doi.org/10.17515/resm2025-557en1202rs
[34] Feng X, Weng C, He X, Han X, Lu L, Ren D, et al. Online State-of-Health Estimation for Li-Ion Battery Using Partial Charging Segment Based on Support Vector Machine. IEEE Trans Veh Technol. 2019;68:8583-8592. https://doi.org/10.1109/TVT.2019.2927120
[35] Deng Y, Ying H, E J, Zhu H, Wei K, Chen J, et al. Feature parameter extraction and intelligent estimation of the State-of-Health of lithium-ion batteries. Energy. 2019;176:91-102. https://doi.org/10.1016/j.energy.2019.03.177
[36] Quin T, Zeng S, Guo J, Skaf Z. A Rest Time-Based Prognostic Framework for State of Health Estimation of Lithium-Ion Batteries with Regeneration Phenomena. Energies. 2016;9:896. https://doi.org/10.3390/en9110896
[37] Cope RC, Podrazhansky Y. The art of battery charging. In: Proceedings of the 14th Annual Battery Conference on Applications and Advances; 1999 Jan 12-15; Long Beach, CA, USA. p. 233-235. https://doi.org/10.1109/BCAA.1999.795996
[38] Ikeya T, Sawada N, Takagi S, Murakami J, Kobayashi K, Sakabe T, et al. Multi-step constant-current charging method for electric vehicle, valve-regulated, lead/acid batteries during night time for load-levelling. J Power Sources. 1998;75:101-107. https://doi.org/10.1016/S0378-7753(98)00102-5
[39] Ikeya T, Sawada N, Murakami J, Kobayashi K, Hattori M, Murotani N, et al. Multi step constant-current charging method for an electric vehicle nickel/metal hydride battery with high-energy efficiency and long cycle life. J Power Sources. 2002;105:6-12. https://doi.org/10.1016/S0378-7753(01)00907-7
[40] Liu Y, Luo Y. Search for an Optimal Rapid-Charging Pattern for Li-Ion Batteries Using the Taguchi Approach. IEEE Trans Ind Electron. 2010;57:3963-3971. https://doi.org/10.1109/TIE.2009.2036020
[41] Vo TT, Chen X, Shen W, Kapoor A. New charging strategy for lithium-ion batteries based on the integration of Taguchi method and state of charge estimation. J Power Sources. 2015;273:413-422. https://doi.org/10.1016/j.jpowsour.2014.09.108
[42] Notten P, het Veld JO, van Beek J. Boostcharging Li-ion batteries: A challenging new charging concept. J Power Sources. 2005;145:89-94. https://doi.org/10.1016/j.jpowsour.2004.12.038

[43] Purushothaman B, Landau U. Rapid Charging of Lithium-Ion Batteries Using Pulsed Currents. J Electrochem Soc. 2006;153:A533-A542. https://doi.org/10.1149/1.2161580
[44] Zhang J, Yu J, Cha C, Yang H. The effects of pulse charging on inner pressure and cycling characteristics of sealed Ni/MH batteries. J Power Sources. 2004;136:180-185. https://doi.org/10.1016/j.jpowsour.2004.05.008
[45] Chen L. A Design of an Optimal Battery Pulse Charge System by Frequency-Varied Technique. IEEE Trans Ind Electron. 2007;54:398-405. https://doi.org/10.1109/TIE.2006.888796
[46] Behara NSR, Rao PS. Vibration energy harvesting using telescopic suspension system for conventional two-wheeler and EV. Res Eng Struct Mater. 2023;9(3):687-707. http://dx.doi.org/10.17515/resm2022.589me1212
[47] Chen Z, Shu X, Li X, Xiao R, Shen J. An optimal charging algorithm for lithium-ion batteries considering temperature rise minimization. In: Chinese Automation Congress (CAC); 2017; Jinan, China. https://doi.org/10.1109/CAC.2017.8243195
[48] Liu YH, Teng JH, Lin YC. Search for an optimal rapid charging pattern for lithium-ion batteries using ant colony system algorithm. IEEE Trans Ind Electron. 2005;52:1328-1336. https://doi.org/10.1109/TIE.2005.855670
[49] Guo Z, Liaw BY, Qiu X, Gao L, Zhang C. Optimal charging method for lithium-ion batteries using a universal voltage protocol accommodating aging. J Power Sources. 2015;274:957-964. https://doi.org/10.1016/j.jpowsour.2014.10.185
[50] Guo Z, Qiu X, Hou G, Liaw BY, Zhang C. State of health estimation for lithium-ion batteries based on charging curves. J Power Sources. 2014;249:457-462. https://doi.org/10.1016/j.jpowsour.2013.10.114
[51] Hu X, Li S, Peng H, Sun F. Charging time and loss optimization for LiNMC and LiFePO4 batteries based on equivalent circuit models. J Power Sources. 2013;239:449-457. https://doi.org/10.1016/j.jpowsour.2013.03.157
[52] Aliev R, Aliev R, Guirimov B, Uyar K. Dynamic data mining technique for rules extraction in a process of battery charging. Appl Soft Comput. 2008;8:1252-1258. https://doi.org/10.1016/j.asoc.2007.02.015
[53] Guo G, Xu P, Bai Z, Zhou S, Xu G, Cao B. Optimization of Ni-MH Battery Fast Charging in Electric Vehicles Using Dynamic Data Mining and ANFIS. In: Advanced Intelligent Computing Theories and Applications. Berlin/Heidelberg: Springer; 2008. p. 468-475. https://doi.org/10.1007/978-3-540-85984-0_56
[54] Petchjatuporn P, Khaehintung N, Sunat K, Sirisuk P, Kiranon W. Implementation of GA-trained GRNN for Intelligent Fast Charger for Ni-Cd Batteries. In: Proceedings of the 2006 CES/IEEE 5th International Power Electronics and Motion Control Conference; 2006 Aug 14-16; Shanghai, China. Vol 1, p. 1-5. https://doi.org/10.1109/IPEMC.2006.4777963
[55] Chen L, Hsu RC, Liu C. A Design of a Grey-Predicted Li-Ion Battery Charge System. IEEE Trans Ind Electron. 2008;55:3692-3701. https://doi.org/10.1109/TIE.2008.928106
[56] Richter F, Kjelstrup S, Vie PJ, et al. Thermal conductivity and internal temperature profiles of Li-ion secondary batteries. J Power Sources. 2017;359:592-600. https://doi.org/10.1016/j.jpowsour.2017.05.045
[57] Dai H, Zhu L, Zhu J. Adaptive Kalman filtering based internal temperature estimation with an equivalent electrical network thermal model for hard-cased batteries. J Power Sources. 2015;293:351-365. https://doi.org/10.1016/j.jpowsour.2015.05.087
[58] Raijmakers LH, Danilov DL, van Lammeren JP, et al. Non-zero intercept frequency: An accurate method to determine the integral temperature of Li-ion batteries. IEEE Trans Ind Electron. 2016;63(5):3168-3178. https://doi.org/10.1109/TIE.2016.2516961
[59] Lee KT, Dai MJ, Chuang CC. Temperature-compensated model for lithium-ion polymer batteries with extended Kalman filter state of- charge estimation for an implantable charger. IEEE Trans Ind Electron. 2018;65(1):589-596. https://doi.org/10.1109/TIE.2017.2721880
[60] Mehne J, Nowak W. Improving temperature predictions for Li-ion batteries: Data assimilation with a stochastic extension of a physically-based, thermo-electrochemical model. J Energy Storage. 2017;12:288-296. https://doi.org/10.1016/j.est.2017.05.013
[61] Guo M, Kim GH, White RE. A three-dimensional multi-physics model for a Li-ion battery. J Power Sources. 2013;240:80-94. https://doi.org/10.1016/j.jpowsour.2013.03.170
[62] Jeon DH, Baek SM. Thermal modeling of cylindrical lithium-ion battery during discharge cycle. Energy Convers Manag. 2011;52(8-9):2973-2981. https://doi.org/10.1016/j.enconman.2011.04.013
[63] Jaguemont J, Omar N, Martel F, et al. Streamline three-dimensional thermal model of a lithium titanate pouch cell battery in extreme temperature conditions with module simulation. J Power Sources. 2017;367:24-33. https://doi.org/10.1016/j.jpowsour.2017.09.028
[64] Lin X, Perez HE, Siegel JB. Online parameterization of lumped thermal dynamics in cylindrical lithium-ion batteries for core temperature estimation and health monitoring. IEEE Trans Control Syst Technol. 2013;21(5):1745-1755. https://doi.org/10.1109/TCST.2012.2217143

[65] Shah K, Vishwakarma V, Jain A. Measurement of multiscale thermal transport phenomena in Li-ion cells: A review. J Electrochem Energy Convers Storage. 2016;13(3):030801. https://doi.org/10.1115/1.4034413
[66] Chen D, Jiang J, Li X. Modelling of a pouch lithium-ion battery using a distributed parameter equivalent circuit for internal non-uniformity analysis. Energies. 2016;9(11):865. https://doi.org/10.3390/en9110865
[67] Muratori M, Canova M, Guezennec Y. A reduced-order model for the thermal dynamics of Li-ion battery cells. IFAC Proc Vol. 2010;43(7):192-197. https://doi.org/10.3182/20100712-3-DE-2013.00190
[68] Kim Y, Mohan S, Siegel SJ. The estimation of temperature distribution in cylindrical battery cells under unknown cooling conditions. IEEE Trans Control Syst Technol. 2014;22(6):2277-2286. https://doi.org/10.1109/TCST.2014.2309492
[69] Hu X, Asgari S, Yavuz I. A transient reduced order model for battery thermal management based on singular value decomposition. In: Proceedings of 2014 IEEE Energy Conversion Congress and Exposition (ECCE); 2014; Pittsburgh. p. 3971-3976. https://doi.org/10.1109/ECCE.2014.6953941
[70] Lin C, Yu Q, Xiong R. A study on the impact of open circuit voltage tests on state of charge estimation for lithium-ion batteries. Appl Energy. 2017;205:892-902. https://doi.org/10.1016/j.apenergy.2017.08.124
[71] Grandjean TR, McGordon A, Jennings PA. Structural identifiability of equivalent circuit models for Li-ion batteries. Energies. 2017;10(1):90. https://doi.org/10.3390/en10010090
[72] Tang SX, Camacho-Solorio L, Wang Y. State-of-charge estimation from a thermal-electrochemical model of lithium-ion batteries. Automatica. 2017;83:206-219. https://doi.org/10.1016/j.automatica.2017.06.030
[73] Li J, Wang L, Lyu C. State of charge estimation based on a simplified electrochemical model for a single LiCoO2 battery and battery pack. Energy. 2017;133:572-583. https://doi.org/10.1016/j.energy.2017.05.158
[74] Wang Y, Zhang C, Chen Z. On-line battery state-of-charge estimation based on an integrated estimator. Appl Energy. 2017;185:2026-2032. https://doi.org/10.1016/j.apenergy.2015.09.015
[75] Acuña DE, Orchard ME. Particle-filtering-based failure prognosis via sigma-points: Application to lithium-ion battery state-of-charge monitoring. Mech Syst Signal Process. 2017;85:827-848. https://doi.org/10.1016/j.ymssp.2016.08.029
[76] Zou C, Manzie C, Nešić D. Multi-time-scale observer design for state-of-charge and state-of-health of a lithium-ion battery. J Power Sources. 2016;335:121-130. https://doi.org/10.1016/j.jpowsour.2016.10.040
[77] Xiong B, Zhao J, Su Y. State of charge estimation of vanadium redox flow battery based on sliding mode observer and dynamic model including capacity fading factor. IEEE Trans Sustain Energy. 2017;8(4):1658-1667. https://doi.org/10.1109/TSTE.2017.2699288
[78] Ye M, Guo H, Cao B. A model-based adaptive state of charge estimator for a lithium-ion battery using an improved adaptive particle filter. Appl Energy. 2017;190:740-748. https://doi.org/10.1016/j.apenergy.2016.12.133
[79] Gehring J, Schütte H. A Hardware-in-the-Loop Test Bench for the Validation of Complex ECU Networks. SAE Technical Paper 2002-01-0801; 2002. https://doi.org/10.4271/2002-01-0801
[80] Schütte H, Wältermann P. Hardware-in-the-Loop Testing of Vehicle Dynamics Controllers - A Technical Survey. SAE Technical Paper 2005-01-1660; 2005. https://doi.org/10.4271/2005-01-1660
[81] Schütte H, Plöger M. Hardware-in-the-Loop Testing of Engine Control Units - A Technical Survey. SAE Technical Paper 2007-01-0500; 2007. https://doi.org/10.4271/2007-01-0500
[82] Kandilli C, Uzel M. Evaluation of annual performance of a photovoltaic thermal system integrated with natural zeolites. Res Eng Struct Mater. 2020;6(4):363-374. https://doi.org/10.17515/resm2020.200en0618
[83] Isella A, Manca D. A framework for the design of battery energy storage systems in Power-to-X processes. J Energy Storage. 2025;123:116744. https://doi.org/10.1016/j.est.2025.116744
[84] Aher P, Deshmukh R, Chavan C, et al. A comprehensive equivalent circuit model of Li-ion batteries for SOC estimation in electric vehicles based on parametric sensitivity analysis. Ionics. 2025;31:287-303. https://doi.org/10.1007/s11581-024-05950-2
[85] Li H, Zhao H, Liu D, Li Z, Hu Q. Electro-thermal coupling modeling and heat generation decoupling analysis of semi-solid-state lithium-ion battery. Electrochim Acta. 2025;512:145455. https://doi.org/10.1016/j.electacta.2024.145455
[86] Mukherjee S, Chowdhury K. State of charge estimation techniques for battery management system used in electric vehicles: a review. Energy Syst. 2025;16:1521-1564. https://doi.org/10.1007/s12667-023-00631-x
[87] Soyoye BD, Bhattacharya I, Anthony Dhason MV, Banik T. State of Charge and State of Health Estimation in Electric Vehicles: Challenges, Approaches and Future Directions. Batteries. 2025;11:32. https://doi.org/10.3390/batteries11010032

[88] Opal-RT. Products [Internet]. Opal-RT website; 2026 [cited 2026 Feb 25]. Available from: http://www.opal-rt.com/product
[89] Casado P, Blanes JM, Garrigós A, Marroquí D, Torres C. Evaluation of commercial Li-Ion 18650 battery cells for deep space applications. J Power Sources. 2025;638:236552. https://doi.org/10.1016/j.jpowsour.2025.236552
[90] Pande AS, Soni BP, Sharma AK. Modeling of one and two RC model and state estimation of Lithium-Ion Battery using Thevenin's equivalent Circuit Model. Procedia Comput Sci. 2025;259:494-503. https://doi.org/10.1016/j.procs.2025.03.351
[91] Chung L, Nixon BA, Yu E, Mylopoulos J. Non-Functional Requirements in Software Engineering. Boston: Kluwer Academic Publishers; 2000. https://doi.org/10.1007/978-1-4615-5269-7
[92] Khaleduzzaman S, Wood A, Srivastava A. Real-Time Hardware-in-the-Loop Modeling and Emulation for Utility-Scale Energy Storage Systems: A Review, Challenges and Path Forward. IEEE J Emerg Sel Top Ind Electron. 2025;6(4):1190-1201. https://doi.org/10.1109/JESTIE.2025.3571436
[93] Marhold C, Rohleder C, Salinesi C, Doerr J. Clarifying Non-Functional Requirements to Improve User Acceptance - Experience at Siemens. In: Proceedings of the 15th International Working Conference, REFSQ 2009; 2009 Jun 8-9; Amsterdam, The Netherlands. https://doi.org/10.1007/978-3-642-02050-6_12
[94] Fleischer C, Sauer DU, Barreras JV, Schaltz E, Christensen AE. Development of software and strategies for Battery Management Testing on HIL Simulator. In: 11th International Conference on Ecological Vehicles and Renewable Energies (EVER); 2016. https://doi.org/10.1109/EVER.2016.7476438
[95] Dutta S, Debnath T, Amitabh K, Chauhan M, Majumder S, De K. Electric Mobility in North East India: Transforming the Region's Transportation Landscape. In: 2025 First International Conference on Advances in Computer Science, Electrical, Electronics, and Communication Technologies (CE2CT); 2025; Bhimtal, Nainital, India. p. 377-382. https://doi.org/10.1109/CE2CT64011.2025.10941116
[96] Kandilli C. Exploring the potential of natural zeolites to enhance solar energy systems: A concise review. Res Des. 2024;1(1):13-21. https://doi.org/10.17515/rede2024-001en1101rv
[97] Ozmen HB, Tanrıverdi B. Concrete paradox: Economic importance, environmental impacts, and the sustainability of concrete material. Res Des. 2025;2(2):66-84. https://doi.org/10.17515/rede2025-008en0801rs
[98] Monaco R, Liu X, Murino T, Cheng X, Nielsen PS. A non-functional requirements-based ontology for supporting the development of industrial energy management systems. J Clean Prod. 2023;414:137614. https://doi.org/10.1016/j.jclepro.2023.137614
[99] Dutta S, Majumder S. Efficient Bi-Directional Charging Solutions for Compact Electric Vehicles for Sustainable Mobility. In: 2024 International Conference on Computer, Electronics, Electrical Engineering & their Applications (IC2E3); 2024; Srinagar Garhwal, Uttarakhand, India. p. 1-6. https://doi.org/10.1109/IC2E362166.2024.10826619
[100] Dutta S, Majumder S, De K. Parameter Sizing in Bi-Directional Charging for Compact EVs. In: 2024 IEEE Silchar Subsection Conference (SILCON 2024); 2024; Agartala, India. p. 1-6. https://doi.org/10.1109/SILCON63976.2024.10910648
[101] Sun B, Zhao X, He X, Ruan H, Zhu Z, Zhou X. Virtual Battery Pack-Based Battery Management System Testing Framework. Energies. 2023;16:680. https://doi.org/10.3390/en16020680
[102] Saleem MU, Shakir M, Usman MR, Bajwa MHT, Shabbir N, Ghahfarokhi PS, et al. Integrating Smart Energy Management System with Internet of Things and Cloud Computing for Efficient Demand Side Management in Smart Grids. Energies. 2023;16:4835. https://doi.org/10.3390/en16124835